

---

# Fast Nonlinear Vector Quantile Regression

---

**Aviv A. Rosenberg**<sup>1,3,†</sup>, **Sanketh Vedula**<sup>1,3,†</sup>, **Yaniv Romano**<sup>1,2</sup>, and **Alex M. Bronstein**<sup>1,3</sup>

<sup>1</sup>Department of Computer Science, Technion

<sup>2</sup>Department of Electrical and Computer Engineering, Technion

<sup>3</sup>Sibylla, UK

{avivr, sanketh, yromano, bron}@cs.technion.ac.il

†Equal Contribution

## Abstract

Quantile regression (QR) is a powerful tool for estimating one or more conditional quantiles of a target variable  $Y$  given explanatory features  $X$ . A limitation of QR is that it is only defined for scalar target variables, due to the formulation of its objective function, and since the notion of quantiles has no standard definition for multivariate distributions. Recently, vector quantile regression (VQR) was proposed as an extension of QR for high-dimensional target variables, thanks to a meaningful generalization of the notion of quantiles to multivariate distributions. Despite its elegance, VQR is arguably not applicable in practice due to several limitations: (i) it assumes a linear model for the quantiles of the target  $Y$  given the features  $X$ ; (ii) its exact formulation is intractable even for modestly-sized problems in terms of target dimensions, number of regressed quantile levels, or number of features, and its relaxed dual formulation may violate the monotonicity of the estimated quantiles; (iii) no fast or scalable solvers for VQR currently exist. In this work we fully address these limitations, namely: (i) We extend VQR to the non-linear case, showing substantial improvement over linear VQR; (ii) We propose vector monotone rearrangement, a method which ensures the estimates obtained by VQR relaxations are monotone functions; (iii) We provide fast, GPU-accelerated solvers for linear and nonlinear VQR which maintain a fixed memory footprint with number of samples and quantile levels, and demonstrate that they scale to millions of samples and thousands of quantile levels; (iv) We release an optimized python package of our solvers as to widespread the use of VQR in real-world applications.

## 1 Introduction

Quantile regression (QR) [16] is a well-known method to estimates a *conditional quantile* of a target variable  $Y$ , given covariates  $X$ . A major limitation of QR is that it deals with a scalar-valued target variable, while many important applications require estimation of vector-valued responses. A trivial approach is to estimate conditional quantiles separately for each component of the vector-valued target. However this assumes statistical independence between targets, a very strong assumption rarely held in practice. Extending QR to high dimensional responses is not straightforward because (i) the notion of quantiles is not trivial to define for high dimensional variables, and indeed multiple definitions of multivariate quantiles exist [5]; (ii) quantile regression is performed by minimizing the *pinball loss* function [16], which is not defined for high dimensional responses.

Seminal works of Carlier et al. [5] and Chernozhukov et al. [10] introduced a notion of quantiles for vector-valued variables, termed *vector quantiles*. Key to their approach is extending the notions of

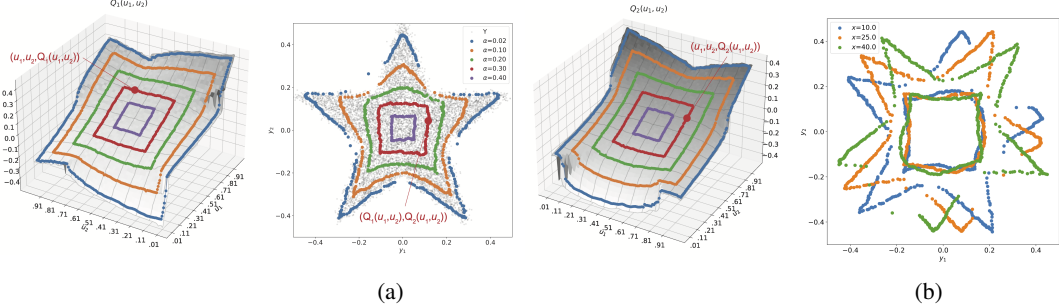


Figure 1: Illustration of vector quantiles of a 2-dimensional star-shaped distribution, where  $T = 50$  quantile levels were estimated in each dimension. (a) Vector quantiles (colored dots) are overlaid on their data distribution (middle). Different colors correspond to  $\alpha$ -contours, each containing  $100 \cdot (1 - 2\alpha)^2$  percent of the data, a generalization of confidence intervals for vector-valued variables. The vector quantile function (VQF)  $Q_{\mathbf{Y}}(\mathbf{u}) = [Q_1(\mathbf{u}), Q_2(\mathbf{u})]^\top$  is co-monotonic with  $\mathbf{u} = (u_1, u_2)$ . The components  $Q_1, Q_2$  of the VQF are shown as surfaces (left, right) with the corresponding vector quantiles overlaid. On  $Q_1$ , increasing  $u_1$  for a fixed  $u_2$  produces a monotonically increasing curve, and vice versa for  $Q_2$ . (b) Conditional vector quantile functions (CVQFs) for a joint distribution of  $(\mathbf{X}, \mathbf{Y})$  where  $\mathbf{Y}|\mathbf{X} = \mathbf{x}$  has a star-shaped distribution rotated by  $\mathbf{x}$  degrees. The CVQF of  $\mathbf{Y}|\mathbf{X} = \mathbf{x}$  changes nonlinearly with the covariates  $\mathbf{x}$ , while e.g.  $\mathbb{E}[\mathbf{Y}|\mathbf{X}]$  remains the same. This demonstrates the challenge of estimating CVQFs from samples of the joint distribution. Two  $\alpha$ -contours are depicted for each  $\mathbf{x}$ . Digital zoom-in recommended.

monotonicity and strong representation of scalar quantile functions to high dimensions, i.e.

$$\text{Co-monotonicity: } (Q_{\mathbf{Y}}(\mathbf{u}) - Q_{\mathbf{Y}}(\mathbf{u}'))^\top (\mathbf{u} - \mathbf{u}') \geq 0, \forall \mathbf{u}, \mathbf{u}' \in [0, 1]^d \quad (1)$$

$$\text{Strong representation: } \mathbf{Y} = Q_{\mathbf{Y}}(\mathbf{U}), \mathbf{U} \sim \mathbb{U}[0, 1]^d \quad (2)$$

where  $\mathbf{Y}$  is a  $d$ -dimensional random variable, and  $Q_{\mathbf{Y}} : [0, 1]^d \mapsto \mathbb{R}^d$  is its vector quantile function.

Moreover, Carlier et al. [5] extended QR to vector-valued targets, which leads to *vector quantile regression* (VQR). This enables estimation of conditional vector quantile functions  $Q_{\mathbf{Y}|\mathbf{X}}$  from samples drawn from  $P_{(\mathbf{X}, \mathbf{Y})}$ , where  $\mathbf{Y}$  is a  $d$ -dimensional target variable and  $\mathbf{X}$  are  $k$ -dimensional covariates. They show that a conditional quantile function  $Q_{\mathbf{Y}|\mathbf{X}}$  which obeys co-monotonicity (1) and strong representation (2) exists and is unique. Under the assumption of a linear specification  $Q_{\mathbf{Y}|\mathbf{X}}(\mathbf{u}; \mathbf{x}) = \mathbf{B}(\mathbf{u})^\top \mathbf{x} + \mathbf{a}(\mathbf{u})$ , they formulate VQR as an optimal transport problem between the measures of  $\mathbf{Y}|\mathbf{X}$  and  $\mathbf{U}$ , with the additional mean-independence constraint  $\mathbb{E}[\mathbf{U}|\mathbf{X}] = \mathbb{E}[\mathbf{X}]$ . Figure 1 provides a visualization of these notions for a two-dimensional target variable. The primal formulation of this problem is large-scale linear program and is thus intractable for modestly-sized problems. A relaxed dual formulation which is amenable to gradient-based solvers exists [7], but results in violations of co-monotonicity.

The first goal of our work is to address the following limitations of Carlier et al. [5, 7]: (i) the linear specification assumption on the conditional quantile function, and (ii) the violation of co-monotonicity when solving the inexact formulation of the VQR problem. The second goal of this work is to make VQR an accessible tool for off-the-shelf usage on large-scale high-dimensional datasets. Currently there is no available solver for the relaxed dual formulation of VQR, which is necessary in order to scale reasonably with problem size. Below we list our contributions.

**Nonlinear VQR.** To address the limitation of linear specification, in Section 5 we propose *nonlinear vector quantile regression*. The key idea is fit a nonlinear embedding function of the input features jointly with the regression coefficients. We demonstrate that nonlinear VQR can model complex conditional quantile functions significantly better than linear VQR.

**Vector monotone rearrangement (VMR).** In Section 4 we propose VMR, which resolves the co-monotonicity violations in estimated conditional vector quantile functions. We solve an optimal transport problem to *rearrange* the vector quantiles such that they satisfy co-monotonicity. It can be viewed as a vector extension to the monotone rearrangement originally proposed by Chernozhukov et al. [9] for scalar quantiles.

**Scalable VQR.** We introduce a highly-scalable solver for linear and nonlinear VQR in Section 3. Our approach, inspired by Genevay et al. [15] and Carlier et al. [7], relies on solving the relaxed dual formulation of the VQR problem. We propose stochastic-gradient-based solvers which maintain a constant memory footprint regardless of problem size. We demonstrate that our solvers can scale to millions of samples and thousands of quantile levels and allow for GPU-acceleration.

**Open-source software package.** We release a feature-rich, well-tested software implementing estimation of vector quantiles, vector ranks, vector quantile contours, linear and nonlinear VQR, and VMR. To the best of our knowledge, this would be the first publicly available tool for estimating conditional vector quantile functions at scale.

## 2 Background

**Notation.** Throughout,  $Y, \mathbf{X}$  denote random variables and vectors, respectively; deterministic scalars, vectors and matrices are denoted as  $y, \mathbf{x}$ , and  $\mathbf{X}$ .  $P_{(\mathbf{X}, Y)}$  denotes the joint distribution of the  $\mathbf{X}$  and  $Y$ .  $\mathbf{1}_N$  denotes an  $N$ -dimensional vector of ones,  $\odot$  denotes the elementwise product, and  $\mathbb{I}\{\cdot\}$  is an indicator. We denote by  $N$  the number of samples,  $d$  the dimension of the target variable,  $k$  the dimension of the covariates, and  $T$  the number of (vector) quantile levels per target dimension.  $Q_{Y|\mathbf{X}}(\mathbf{u}; \mathbf{x})$  is the conditional (vector) quantile function of the variable  $Y|\mathbf{X}$  evaluated at the (vector) quantile level  $\mathbf{u}$  for  $\mathbf{X} = \mathbf{x}$ .

**Quantile Regression.** The goal of QR is to estimate the quantile of a variable  $Y|\mathbf{X}$ . Under the assumption of a linear model of the latter, and given  $u \in (0, 1)$ , QR amounts to solving  $(\mathbf{b}_u, a_u) = \arg \min_{\mathbf{b}, a} \mathbb{E}_{(\mathbf{X}, Y)} [\rho_u(Y - \mathbf{b}^\top \mathbf{X} - a)]$ , where  $\mathbf{b}_u^\top \mathbf{x} + a_u$  is the  $u$ -th quantile of  $Y|\mathbf{X} = \mathbf{x}$ , and  $\rho_u(z)$ , known as the *pinball loss*, is given by  $\rho_u(z) = \max\{0, z\} + (u - 1)z$ . Solving this problem produces an estimate of  $Q_{Y|\mathbf{X}}$  for a single quantile level  $u$ . In order to estimate the full conditional quantile function (CQF)  $Q_{Y|\mathbf{X}}(u)$ , the problem must be solved at all levels of  $u$  with additional monotonicity constraints, since any quantile function is strictly non-decreasing in  $u$ . The discrete form QR for estimating the CQF, sampled at  $T$  quantile levels, from  $N$  samples  $\{\mathbf{x}_i, y_i\}_{i=1}^N \sim P_{(\mathbf{X}, Y)}$ , can be written as

$$\begin{aligned} \min_{\mathbf{B}, \mathbf{a}} \quad & \sum_u \sum_{i=1}^N \rho_u(y_i - \mathbf{b}_u^\top \mathbf{x}_i - a_u) \\ \text{s.t. } \forall i, u' \geq u \implies & \mathbf{b}_{u'}^\top \mathbf{x}_i + a_{u'} \geq \mathbf{b}_u^\top \mathbf{x}_i + a_u, \end{aligned} \tag{3}$$

where  $\mathbf{B}$  and  $\mathbf{a}$  aggregate all the  $\mathbf{b}_u$  and  $a_u$ , respectively. We refer to eq. (3) as *simultaneous linear quantile regression* (SLQR). This problem is undefined for a vector-valued  $Y$ , due to the definition of the pinball loss  $\rho_u(z)$ , as well as the inherently 1d formulation of the monotonicity constraints.

**Optimal Transport Formulation.** Carlier et al. [5] showed that SLQR (3) can be equivalently written as an optimal transport (OT) problem between the target variable and the quantile levels, with an additional constraint of mean independence. Given  $N$  data samples arranged as  $\mathbf{y} \in \mathbb{R}^N$ ,  $\mathbf{X} \in \mathbb{R}^{N \times k}$ ,  $\bar{\mathbf{x}} = \frac{1}{N} \mathbf{1}_N^\top \mathbf{X}$ , and  $T$  quantile levels denoted by  $\mathbf{u} = [\frac{1}{T}, \frac{2}{T}, \dots, 1]^\top$  we can write,

$$\begin{aligned} \max_{\mathbf{\Pi} \geq 0} \quad & \mathbf{u}^\top \mathbf{\Pi} \mathbf{y} \\ \text{s.t. } \mathbf{\Pi}^\top \mathbf{1}_T = \boldsymbol{\nu} \quad & \\ \mathbf{\Pi} \mathbf{1}_N = \boldsymbol{\mu} \quad & [\mathbf{D}^{-\top} \mathbf{a}] \\ \mathbf{\Pi} \mathbf{X} = \frac{1}{T} \mathbf{1}_T \bar{\mathbf{x}} \quad & [\mathbf{D}^{-\top} \mathbf{B}] \end{aligned} \tag{4}$$

where  $\mathbf{\Pi}$  is the transport map between quantile levels  $\mathbf{u}$  and samples of  $Y|\mathbf{X}$ , with marginals  $\boldsymbol{\nu} = \frac{1}{N} \mathbf{1}_N$  and  $\boldsymbol{\mu} = \frac{1}{T} \mathbf{1}_T$ . The dual variables (appearing in square brackets) can be written as  $\boldsymbol{\alpha} = \mathbf{D}^{-\top} \mathbf{a}$  and  $\boldsymbol{\beta} = \mathbf{D}^{-\top} \mathbf{B}$ , where  $\mathbf{D}^\top$  is a first-order finite differences matrix, and  $\mathbf{a} \in \mathbb{R}^T$ ,  $\mathbf{B} \in \mathbb{R}^{T \times k}$  contain the regression coefficients for all quantile levels. Refer to appendix A for a full derivation of the connection between SLQR (3) and OT (4).

**Vector Quantile Regression.** Although the OT formulation for SLQR (4) is specified between 1d measures, this formulation is immediately extensible to higher dimensions. Given vector-valued targets  $\mathbf{y}_i \in \mathbb{R}^d$  arranged in  $\mathbf{Y} \in \mathbb{R}^{N \times d}$ , their vector quantiles are also in  $\mathbb{R}^d$ . The vector quantile levels are sampled on a uniform grid on  $[0, 1]^d$  with  $T$  evenly spaced points in each dimension,

resulting in a total of  $T^d$   $d$ -dimensional vector quantile levels, arranged as  $\mathbf{U} \in \mathbb{R}^{T^d \times d}$ . Notice that the OT objective can be written as  $\mathbf{u}^\top \mathbf{\Pi} \mathbf{y} = \sum_{t=1}^T \sum_{i=1}^N \Pi_{t,i} u_t y_i = \mathbf{\Pi} \odot \mathbf{S}$ , where  $\mathbf{S} \in \mathbb{R}^{T \times N}$ . This can be naturally extended to  $d > 1$  by defining the pairwise inner-product matrix  $\mathbf{S} = \mathbf{U} \mathbf{Y}^\top \in \mathbb{R}^{T^d \times N}$ . Appendix A details how the regression coefficients  $\mathbf{a} \in \mathbb{R}^{T^d}$  and  $\mathbf{B} \in \mathbb{R}^{T^d \times k}$  are obtained from the dual variables in the high-dimensional case. The result is a  $d$ -dimensional conditional vector quantile function (CVQF),  $Q_{\mathbf{Y}|\mathbf{X}}(\mathbf{u}; \mathbf{x})$ , defined for any  $\mathbf{X} = \mathbf{x}$ , and discretized at each quantile level  $\mathbf{u} \in [0, 1]^d$ . Note that the CVQF is monotonic in the sense defined by eq. (1) for each value of  $\mathbf{x}$ . Figure 1 presents visual intuition about the CVQF. Refer to Appendix B for a detailed explanation.

### 3 Scalable VQR

Numerous works proposed fast solvers for variants of OT problems. A common approach for scaling OT to larger problems is to introduce an entropic regularization term  $-\varepsilon \sum_{i,j} \Pi_{i,j} \log \Pi_{i,j}$  to the OT objective. As shown by Cuturi [11], this regularized formulation allows using the Sinkhorn algorithm which provides significant speedup. Other solvers have been proposed for OT variants with application-specific regularization terms on  $\mathbf{\Pi}$  [13, 19, 1]. These solvers are, however, not applicable in our case due to the additional mean-independence constraint. Solving a linear program with general-purpose solvers has complexity that is cubic in the number of optimization variables and constraints. The primal VQR problem (5) has  $T^d \cdot N$  variables and  $T^d \cdot (k+1) + N$  constraints; employing such solvers is thus intractable for modestly-sized VQR problems. Another approach for solving OT is to solve its dual formulation. Solving OT via its regularized dual allows to encode the additional mean-independence constraint, as shown by the recent work of Carlier et al. [7]. Genevay et al. [15] showed that a relaxed dual version of the standard OT problem is amenable to stochastic optimization and can thus scale to large number of samples. Inspired by these works, we implement a highly-scalable solver for VQR which employs stochastic gradients in both samples ( $N$ ) and quantile levels ( $T^d$ ). Equations (5) and (6) present the OT primal and dual formulations of VQR respectively, where the mean-independence constraint becomes<sup>1</sup>  $\mathbf{\Pi} \mathbf{X} = \mathbf{0}$ .

$$\begin{aligned} \max_{\mathbf{\Pi} \geq 0} \quad & \mathbf{U}^\top \mathbf{\Pi} \mathbf{Y} \\ \text{s.t.} \quad & \mathbf{\Pi}^\top \mathbf{1}_{T^d} = \boldsymbol{\nu} \quad [\boldsymbol{\psi}] \quad (5) \\ & \mathbf{\Pi} \mathbf{1}_N = \boldsymbol{\mu} \quad [\boldsymbol{\varphi}] \\ & \mathbf{\Pi} \mathbf{X} = \mathbf{0} \quad [\boldsymbol{\beta}] \end{aligned} \quad \begin{aligned} \min_{\boldsymbol{\psi}, \boldsymbol{\varphi}, \boldsymbol{\beta}} \quad & \sum_{j=1}^N \psi_j \nu_j + \sum_{i=1}^{T^d} \varphi_i \mu_i \\ \text{s.t.} \quad & \forall i, j : \\ & \varphi_i + \boldsymbol{\beta}_i^\top \mathbf{x}_j + \psi_j \geq \mathbf{u}_i^\top \mathbf{y}_j \quad [\mathbf{\Pi}] \end{aligned} \quad (6)$$

Here  $\boldsymbol{\psi} \in \mathbb{R}^N$ ,  $\boldsymbol{\varphi} \in \mathbb{R}^{T^d}$ , and  $\boldsymbol{\beta} \in \mathbb{R}^{T^d \times k}$  are the dual variables, and  $\boldsymbol{\mu} = \frac{1}{T^d} \mathbf{1}_{T^d}$ ,  $\boldsymbol{\nu} = \frac{1}{N} \mathbf{1}_N$  are the marginals. After solving, the CVQF is  $Q_{\mathbf{Y}|\mathbf{X}}(\mathbf{u}; \mathbf{x}) = \nabla_{\mathbf{u}} \{ \boldsymbol{\beta}^\top \mathbf{x} + \boldsymbol{\varphi} \}$  as detailed in appendix A.

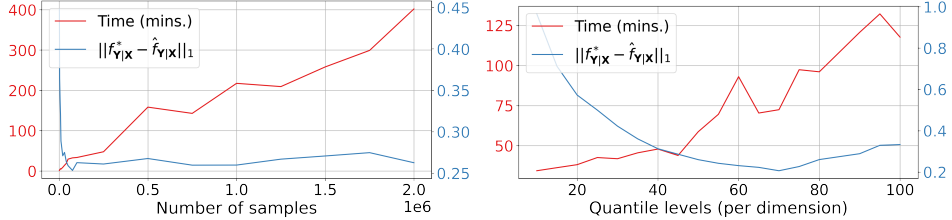
The relaxed formulation of eq. (6) is

$$\min_{\boldsymbol{\psi}, \boldsymbol{\beta}} \sum_{j=1}^N \psi_j \nu_j + \varepsilon \sum_{i=1}^{T^d} \mu_i \log \left( \sum_{j=1}^N \exp \left( \frac{1}{\varepsilon} (\mathbf{u}_i^\top \mathbf{y}_j - \boldsymbol{\beta}_i^\top \mathbf{x}_j - \psi_j) \right) \right), \quad (7)$$

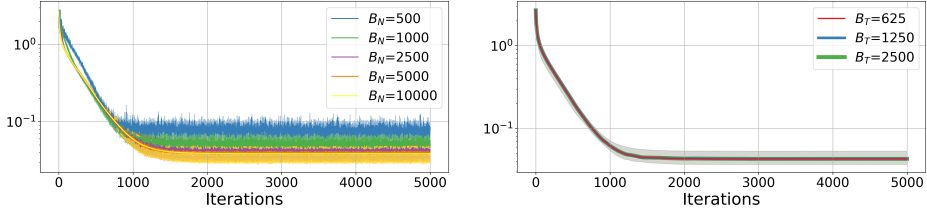
where  $\varepsilon$  controls the exactness of the the objective; as  $\varepsilon$  decreases, the relaxed dual more closely approximates the exact dual. In practice we perform VQR by solving eq. (7) using stochastic gradient based optimization. Although the relaxed dual formulation for VQR was proposed by Carlier et al. [7], they did not show SGD-based solvers for this problem. Furthermore, as we will show, this approach might result in a quantile function that violates co-monotonicity, due to relaxing the constraints. In Section 4 we show how this limitation can be overcome. Appendix A presents the derivation of eq. (7) from eq. (6), and that eq. (7) is equivalent to the dual of an entropic-regularized eq. (5).

The relaxed dual formulation of VQR (7) involves only  $T^d \cdot k + N$  optimization variables. However, calculating the objective requires materializing two  $T^d \times N$  inner-product matrices. Thus, the memory footprint grows exponentially with  $d$  and polynomially with  $T$ . Although the objective is amenable to GPU-based acceleration, as it involves only dense-matrix multiplications and pointwise operations, the need to materialize matrices of size  $T^d \times N$  severely limits the problem size which can be feasibly solved on general-purpose GPUs. This problem is exacerbated when  $\mathbf{X}$  is high-dimensional, as it must also be kept in memory.

<sup>1</sup>under the assumption of  $\mathbb{E} [\mathbf{X}] = \mathbf{0}$  which can be assumed without loss of generality; in practice one can always standardize the features to have zero mean.



(a) Scale: VQR performance when scaling  $N$  and  $T$ . Computed on MVN dataset with  $d = 2$  and  $k = 10$ . The blue curve shows the KDE-L1 metric, defined in section 6. Left: Sweeping over  $N$ ;  $T = 50$  and  $B_N = 50k$ . Right: Sweeping over  $T$ ;  $N = 100k$ , and  $B_T = 2500$ .



(b) Optimization: Effect of batch sizes  $B_N$  and  $B_T$ . Computed on MVN dataset with  $d = 2$  and  $k = 1$ . The vertical axis is the QFD metric defined in section 6. Left: Sweeping over  $B_N$ ;  $T = 25$ . Right: Sweep over  $B_T$ ;  $T = 50$  produces  $50^2$  total levels.

Figure 2: Scale and Optimization performance of our VQR solver.

**SGD-based VQR.** To attain a constant memory footprint w.r.t.  $T$  and  $N$ , we adapt the approach of Genevay et al. [15], for the VQR problem. We sample data points from  $\{(\mathbf{x}_j, \mathbf{y}_j)\}_{j=1}^N$  together with vector quantile levels from  $\{\mathbf{u}_i\}_{i=1}^{T^d}$  and evaluate eq. (7) on these samples. When sampling quantile levels, we select the corresponding entries from  $\boldsymbol{\beta}$  and  $\boldsymbol{\mu}$ ; likewise, when sampling data points, we select the corresponding entries from  $\boldsymbol{\psi}$ . Thus, by setting a fixed batch size for both data points and levels, we solve VQR with a constant memory footprint irrespective of problem size (fig. 2a). Moreover, we observe that in practice, using SGD adds only negligible optimization error to the solution, with smaller batches producing more error as expected (fig. 2b). Refer to Appendix D for further implementation details.

#### 4 Vector Monotone Rearrangement

As explained above, solving eq. (7) may lead to violation of co-monotonicity in  $Q_{Y|X}$ , due to the relaxation of the exact constraints in eq. (6). This is analogous to the quantile crossing problem in the scalar case, which can also manifest when QR is performed separately for each quantile level [9]. See fig. 3a for an example.

Consider the case of scalar quantiles, i.e.,  $d = 1$ . Denote  $\hat{Q}_{Y|X}(u; \mathbf{x})$  as an estimated conditional quantile function (CQF), which may be non-monotonic in  $u$  due to estimation error. Chernozhukov et al. [9] proposed to convert  $\hat{Q}_{Y|X}(u; \mathbf{x})$  into a monotonic  $\tilde{Q}_{Y|X}(u; \mathbf{x})$  through rearrangement. Consider a random variable defined as  $\hat{Y}|X := \hat{Q}_{Y|X}(U; \mathbf{x})$  where  $U \sim \mathbb{U}[0, 1]$ . Since  $\hat{Q}_{Y|X}(U; \mathbf{x})$  might not be a CQF, denote the CQF of  $\hat{Y}|X$  as  $Q_{\hat{Y}|X}(u; \mathbf{x})$ . The CDF and inverse CDF of  $\hat{Y}|X$  are,  $F_{\hat{Y}|X}(y; \mathbf{x}) = \int_0^1 \mathbb{I}\{\hat{Q}_{Y|X}(u; \mathbf{x}) \leq y\}$ , and  $Q_{\hat{Y}|X}(u; \mathbf{x}) = \inf\{y : F_{\hat{Y}|X}(y; \mathbf{x}) \geq u\}$ .  $Q_{\hat{Y}|X}(u; \mathbf{x})$  is necessarily monotonic, and Chernozhukov et al. [9] further showed that it is no worse an estimator for the true CQF,  $Q_{Y|X}(u; \mathbf{x})$ , than  $\hat{Q}_{Y|X}(u; \mathbf{x})$  in the  $L_p$ -norm sense. In practice, this rearrangement is performed in the scalar case by sorting the discrete estimated CQF.<sup>2</sup>

Here, we extend the notion of rearrangement to the case of  $d > 1$ . As before, define  $\hat{Y}|X := \hat{Q}_{Y|X}(\mathbf{U}; \mathbf{x})$  where  $\mathbf{U} \sim \mathbb{U}[0, 1]^d$ , and  $\hat{Q}_{Y|X}(u; \mathbf{x})$  is the estimated CVQF. If it is not co-monotonic,

<sup>2</sup>Rearrangement has no effect if  $\hat{Q}_{Y|X}(u; \mathbf{x})$  is already monotonic.

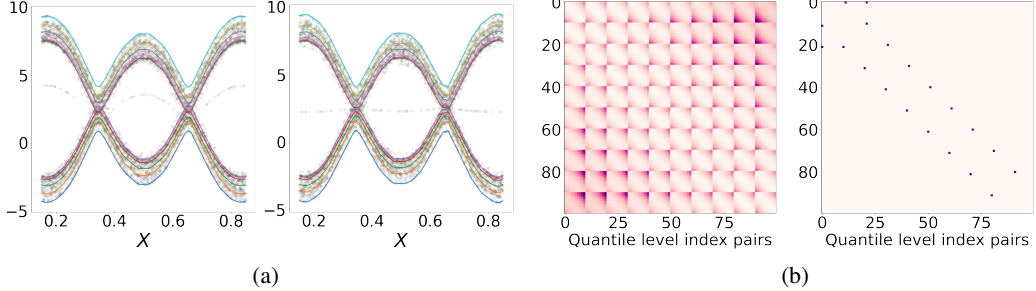


Figure 3: Monotone rearrangement and monotonicity violations in 1d and 2d. (a) The quantile crossing problem in 1d. Gray points: samples the synthetic glasses dataset [3]; Colored lines: quantile curves for different levels obtained with nonlinear VQR, fitted with  $N = 10k$ ,  $T = 100$ . Left: Without VMR, quantile crossings are present. Right: With VMR, no quantile crossings. (b) Left: co-monotonicity matrix, showing the value of  $(\mathbf{u}_i - \mathbf{u}_j)^\top (Q(\mathbf{u}_i) - Q(\mathbf{u}_j))$  for all  $i, j$ , after fitting VQR without VMR with  $d = 2$ ,  $T = 10$  on the MVN dataset. Right: quantile-level pairs  $i, j$  where co-monotonicity is violated. VMR resolves all these violations. Digital zoom-in recommended.

as defined by eq. (1), we can compute a co-monotonic  $Q_{\widehat{\mathbf{Y}}|\mathbf{X}}(\mathbf{u}; \mathbf{x})$  by calculating the vector quantiles of  $\widehat{\mathbf{Y}}|\mathbf{X} = \mathbf{x}$ , separately for each  $\mathbf{x}$ . We emphasize that this amounts to solving the simpler *vector quantile estimation* problem for a specific  $\mathbf{x}$ , as opposed to the vector quantile regression problem.

Let  $\widehat{\mathbf{Q}} = [\widehat{\mathbf{q}}_j]_j \in \mathbb{R}^{T^d \times d}$  be the estimated CVQF  $\widehat{Q}_{\mathbf{Y}|\mathbf{X}}(\mathbf{u}; \mathbf{x})$  sampled at  $T^d$  levels  $\mathbf{U} = [\widehat{\mathbf{u}}_i]_i \in \mathbb{R}^{T^d \times d}$  by solving VQR. To obtain  $Q_{\widehat{\mathbf{Y}}|\mathbf{X}}(\mathbf{u}; \mathbf{x})$  sampled at  $\mathbf{U}$  we solve

$$\max_{\pi_{i,j} \geq 0} \sum_{i,j=1}^{T^d} \pi_{i,j} \mathbf{u}_i^\top \widehat{\mathbf{q}}_j \quad \text{s.t.} \quad \mathbf{\Pi}^\top \mathbf{1} = \mathbf{\Pi} \mathbf{1} = \frac{1}{T^d} \mathbf{1}, \quad (8)$$

and then compute  $\widetilde{\mathbf{Q}} = T^d \cdot \mathbf{\Pi} \widehat{\mathbf{Q}}$ . We define this procedure as *vector monotone rearrangement* (VMR). The existence and uniqueness of a co-monotonic function, mapping between the measures of  $\mathbf{U}$  and  $\widehat{Q}_{\mathbf{Y}|\mathbf{X}}(\mathbf{U}; \mathbf{x})$  is due to the theoretical results by Brenier [4] and McCann [17].<sup>3</sup> VMR can be interpreted as ‘‘vector sorting’’ of the discrete CVQF estimated with VQR, since it effectively permutes the entries of  $\widehat{\mathbf{Q}}$  such that the resulting  $\widetilde{\mathbf{Q}}$  is co-monotonic with  $\mathbf{U}$ . Note that eq. (8) is an OT problem with the inner-product matrix as the ground cost, and simple constraints on the marginals of the transport map  $\mathbf{\Pi}$ . Thus, VMR (8) is significantly simpler to solve *exactly* than VQR (5). We leverage fast, off-the-shelf OT solvers from the POT library [14, 2]. We use VMR as a post-processing step, performed after the estimated CVQF  $\widehat{Q}_{\mathbf{Y}|\mathbf{X}}(\mathbf{u}; \mathbf{x})$  is evaluated for a specific  $\mathbf{x}$ .

Figure 3 demonstrates the quantile crossing problem in 1d and 2d. In the case of 1d, quantile crossings before and after VMR correction can be readily visualized. Although for  $d = 1$  the crossings could be resolved by sorting, our method works for any  $d$ . For  $d > 1$ , monotonicity violations manifest as  $(\mathbf{u}_i - \mathbf{u}_j)^\top (Q(\mathbf{u}_i) - Q(\mathbf{u}_j)) < 0$ , as shown in fig. 3b. These violations are completely eliminated by VMR, since by definition the exact VMR objective (8) results in co-monotonicity.

## 5 Nonlinear VQR

Carlier et al. [5] proved the existence and uniqueness of a conditional quantile function which satisfies strong representation, i.e.,  $\mathbf{Y}|(\mathbf{X} = \mathbf{x}) = Q_{\mathbf{Y}|\mathbf{X}}(\mathbf{U}; \mathbf{x})$ , and is co-monotonic w.r.t.  $\mathbf{U}$ . In order to estimate this function from finite samples, they further assumed a linear specification in both  $\mathbf{u}$  and  $\mathbf{x}$ , given by the model  $Q_{\mathbf{Y}|\mathbf{X}}^L(\mathbf{u}; \mathbf{x}) = \mathbf{B}(\mathbf{u})^\top \mathbf{x} + \mathbf{a}(\mathbf{u})$ . This results in the OT problem with the mean-independence constraint presented in eq. (5). However, in practice and with real-world datasets, there is no reason to assume that such a specification is valid. In cases where the true CVQF is a non-linear function of  $\mathbf{x}$  this model is mis-specified and the estimated CVQF does not satisfy strong representation. We address this limitation by modelling the CVQF as a non-linear function of the covariates parametrized by  $\theta$ , i.e.,  $Q_{\mathbf{Y}|\mathbf{X}}^{NL}(\mathbf{u}; \mathbf{x}) = \mathbf{B}(\mathbf{u})^\top g_\theta(\mathbf{x}) + \mathbf{a}(\mathbf{u})$ . We fit  $\theta$  *jointly* with the

<sup>3</sup>Refer to Theorem 2.32 in Villani [21] for a proof.

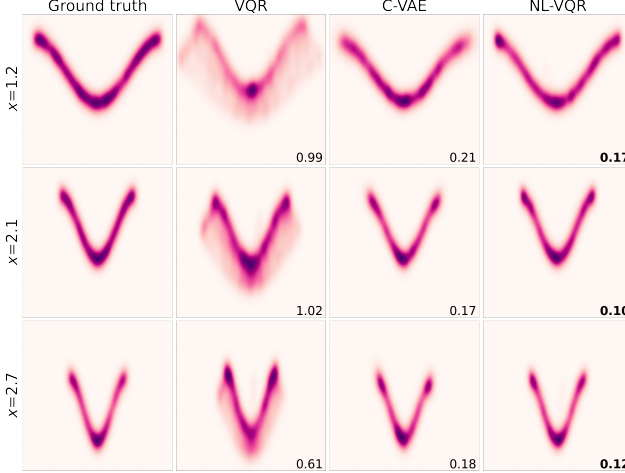


Figure 4: Comparison of kernel-density estimates of samples drawn from linear VQR, CVAE, and nonlinear VQR (NL-VQR), trained on the conditional-banana dataset. Models were trained with  $N = 20k$  samples; for VQR  $T = 50$  was used. Numbers depict the KDE-L1 metrics defined in section 6. Lower is better; nonlinear VQR outperforms other methods.

regression coefficients  $\mathbf{B}, \mathbf{a}$ . The rationale is to parametrize an embedding  $g_{\theta}(\mathbf{x})$  such that the model is  $Q_{\mathbf{Y}|\mathbf{X}}^{NL}$  is better specified than  $Q_{\mathbf{Y}|\mathbf{X}}^L$  in the sense of strong representation.

Encoding this nonlinear CVQF model into the exact formulations of VQR (eqs. (5) and (6)) will no longer result in a linear program. Thus, our approach is to encode this model into the relaxed dual formulation by minimizing the following modified objective,

$$\min_{\psi, \beta, \theta} \sum_{j=1}^N \psi_j \nu_j + \varepsilon \sum_{i=1}^{T^d} \mu_i \log \left( \sum_{j=1}^N \exp \left( \frac{1}{\varepsilon} (\mathbf{u}_i^\top \mathbf{y}_j - \beta_i^\top g_{\theta}(\mathbf{x}_j) - \psi_j) \right) \right) \quad (9)$$

which we optimize with gradient descent using the approach described in section 3. Because the relaxed dual formulation assumes zero-mean covariates, we must ensure that  $g_{\theta}$  produces zero-mean outputs per batch.

A crucial advantage of our nonlinear CVQF model is that  $g_{\theta}$  may embed  $\mathbf{x} \in \mathbb{R}^k$  into a different dimension,  $k' \neq k$ . This means that VQR can be performed, e.g., on a lower-dimensional projection of  $\mathbf{x}$  or on a “lifted” higher-dimensional representation. For a low-dimensional  $\mathbf{X}$  which has a highly-nonlinear relationship with the target  $\mathbf{Y}$ , lifting it into a higher dimension could result in the linear regression model (with coefficients  $\mathbf{B}$  and  $\mathbf{a}$ ) to be well-specified. Conversely, for high-dimensional  $\mathbf{X}$  which has intrinsic low-dimensionality (e.g., an image),  $g_{\theta}$  may encode a projection operator which has inductive bias, and thus exploits the intrinsic structure of the feature space. This allows one to choose a  $g_{\theta}$  suitable for the problem at hand, for example, a convolutional neural network in case of an image or a graph neural network if  $\mathbf{x}$  lives on a graph.

**Simultaneous Quantile Regression (SQR).** SQR is the task of simultaneously resolving multiple conditional quantiles of a scalar variable, i.e. a possibly non-linear version of eq. (3). Nonlinear SQR has been well-studied, and multiple approaches have been proposed [3, 20]. We emphasize that SQR is in fact a special case of NL-VQR (9) when  $d = 1$ . Since the NL-VQR objective directly emerges from the pinball loss with monotonicity constraints, minimizing (9) promotes monotonicity of the scalar conditional quantiles. As demonstrated in Figure 3a, using NL-VQR together with VMR results in CQFs which are monotonic, i.e., non-crossing; thus, when  $d = 1$ , NL-VQR provides a simple and scalable approach for performing SQR.

**Prior attempts at nonlinear high-dimensional quantiles.** Feldman et al. [12] proposed an approach for constructing high-dimensional confidence regions, based on a conditional variational autoencoder (CVAE). A crucial limitation of this work is that it does not infer the conditional vector quantile function; their resulting confidence regions are not guaranteed to be quantile contours (see fig. 1a), e.g. because they do not satisfy the defining properties of vector quantiles (eqs. (1) and (2)).

## 6 Experiments

In all experiments we use the synthetic datasets named MVN, conditional-banana and synthetic glasses. We evaluate using the following metrics: (i) KDE-L1, an estimate of distance between

distributions; (ii) QFD, a distance measured between estimated quantile functions; (iii) Inverse CVQF entropy; (iv) Monotonicity violations. The first three metrics serve as a measure of strong representation (2), while the fourth measures co-monotonicity (1). The datasets and evaluation metrics are detailed in Appendix C. Additional experiment results can also be found in Appendix C.

## 6.1 Scale and Optimization

**Scalability.** To demonstrate the scalability of our VQR solver and its applicability to large problems, we solved VQR under multiple increasing values of  $N$  and  $T$ , while keeping all other data and training settings fixed, and measured both wall time and KDE-L1. We used up to  $N = 2 \cdot 10^6$  data points,  $d = 2$  dimensions, and  $T = 100$  levels per dimension ( $T^d = 100^2$  levels in total), while sampling both data points and quantile levels stochastically, thus keeping the memory requirement fixed throughout. This enabled us to run the experiment on a commodity 2080Ti GPU with 11GB of memory. Figure 2a presents these results. Runtime increases linearly with  $N$  and quadratically with  $T$ , as can be expected for  $d = 2$ . KDE-L1 generally decreases and then plateaus when increasing  $N$  and  $T$ , showcasing improved accuracy in distribution estimation. To the best of our knowledge, this is the first time that large-scale VQR has been demonstrated.

**Optimization.** To evaluate our SGD-based optimization, we solved VQR under different batch sizes of data points and quantile levels, denoted as  $B_N$  and  $B_T$  respectively. We measured the QFD metric, averaged over 100 evaluation  $x$  values. These results are presented in Figure 2b. As expected, the error increases as  $B_N$  decreases. However, even for the smallest  $B_N$  we achieve less than 10% error. Conversely, we find that batching quantiles level has negligible effect on the optimization error.

## 6.2 Nonlinear VQR

To demonstrate the effectiveness of nonlinear VQR, we use the conditional-banana and synthetic glasses datasets, where the assumption of a linear CVQF is violated.

**CVAE baseline.** We use the CVAE implementation of Feldman et al. [12]<sup>4</sup> as a strong baseline for estimating the conditional distribution of  $\mathbf{Y}|\mathbf{X}$ . We emphasize that this model only allows sampling from the estimated conditional distribution; it does not estimate quantiles, while VQR allows both. Thus, we could compare VQR with CVAE only on the KDE-L1 metric, which is computed on samples. To the best of our knowledge, besides VQR there is no other generative model capable of estimating CVQFs.

**Conditional-banana experiment.** We draw  $N = 20k$  samples from  $P_{(\mathbf{X}, \mathbf{Y})}$  and fit  $T = 50$  quantile levels per dimension ( $d = 2$ ) for linear and nonlinear VQR (NL-VQR). Evaluation is performed by measuring all aforementioned metrics on 4000 evaluation samples from 20 true conditional distributions, conditioned on  $x = [1.1, 1.2, \dots, 3.0]$ . For NL-VQR, as  $g_\theta$  we use a small MLP with three hidden layers of size (2, 10, 20) and a ReLU non-linearity. Thus  $g_\theta$  lifts  $\mathbf{X}$  into 20 dimensions on which VQR is performed. Further training details are provided in appendix C.

**Results.** The results of the conditional-banana experiment, comparing VQR, NL-VQR and CVAE, are presented in Figure 4 and Table 1. We evaluated all methods using the KDE-L1 metric. The Entropy and QFD metrics were evaluated only on VQR and NL-VQR, because CVAE does not produce quantile functions. The metrics are averaged over the 20 evaluation  $x$  values. Two-dimensional KDEs of conditional distributions for three values of  $x$  are shown for each method in Figure 4. Qualitatively, both NL-VQR and CVAE produce visually compelling estimations of the ground truth, when compared to VQR. This clearly indicates that the linear VQR model is mis-specified for this data. This is further corroborated by the entropy metric, presented in Table 1. The entropy of the inverse CVQF is lower for linear VQR, indicating non-uniformity and therefore mis-specification. Although visually NL-VQR and CVAE produced similar qualitative results, in terms of the KDE-L1 metrics, NL-VQR outperforms CVAE by 23%. Furthermore, in terms of QFD, nonlinear VQR results in 70% lower error. These results highlight that nonlinear VQR is significantly more effective at estimating CVQFs compared to VQR. Another point of note is that the CVAE model required 1 hour to train, while VQR and NL-VQR were trained within less than 4 minutes. In other words, NL-VQR performs better than CVAE with an order of magnitude speedup in training time, and better than VQR while requiring similar runtime. Finally, the CVQFs estimated with VQR and NL-VQR are post-processed with VMR. Zero violations of co-monotonicity exist in the obtained CVQFs.

<sup>4</sup> Available at <https://github.com/Shai128/mqr>

Table 1: Quantitative evaluation of linear VQR, CVAE and nonlinear VQR on the conditional-banana dataset. Evaluated on  $N = 4000$  samples with  $T = 50$  levels per dimension. The KDE-L1, QFD and Entropy metrics are defined in section 6. Arrows  $\uparrow/\downarrow$  indicate when higher/lower is better; Numbers are mean  $\pm$  st.d. Reference entropy is obtained by uniformly sampling the 2d quantile grid.

		CVAE	VQR	NL-VQR
KDE-L1	$\downarrow$	$0.175 \pm 0.021$	$0.873 \pm 0.175$	<b><math>0.135 \pm 0.024</math></b>
Quantile Function Distance (QFD)	$\downarrow$	-	$0.179 \pm 0.034$	<b><math>0.055 \pm 0.023</math></b>
Inverse CVQF Entropy (Ref: 0.70)	$\uparrow$	-	$0.309 \pm 0.077$	<b><math>0.560 \pm 0.014</math></b>
Train time (min)	$\downarrow$	60	<b>3.5</b>	4

## 7 Software

We provide our VQR solvers as part of a robust, well-tested python package, `vqr`<sup>5</sup>. As demonstrated in Figure 2a, our package implements fast solvers with support for GPU-acceleration and has a familiar `sklearn`-style API. It supports any number of dimensions for both input features ( $k$ ) and target variables ( $d$ ), and allows for arbitrary neural networks to be used as the learned nonlinear feature transformations,  $g_\theta$ . The package provides tools for estimating vector quantiles, vector ranks, vector quantile contours, and performing VMR as a refinement step after fitting VQR. We provide `jupyter` notebooks with examples as supplementary material. To the best of our knowledge, this would be the first publicly available tool for estimating conditional vector quantile functions at scale.

## 8 Conclusion

In this work we proposed non-linear vector quantile regression, in order to overcome a key limitation of VQR, namely the assumption that the vector quantile function is linear in  $\mathbf{X}$ . Our approach allows, e.g., modelling conditional quantiles when  $\mathbf{X}$  is high dimensional by embedding it into a lower-dimensional space, where VQR is both better specified and faster to compute. We further demonstrated that we can solve VQR at scale, by using a custom solver for the relaxed dual of the VQR problem. As far as we know, large scale estimation of conditional or even unconditional vector quantiles has not been shown prior to this work. Moreover, we resolved the issue of high-dimensional quantile crossings by applying a refinement step for estimated CVQFs, which we called vector monotone rearrangement (VMR).

**Limitations.** An important limitation of our approach is that it does not separate the non-linearity per quantile level, i.e., we have the same non-linear transformation  $g_\theta(\mathbf{x})$  for all levels  $\mathbf{u}$ . Also, though our approach is highly scalable, it still suffers from the curse of dimensionality, especially in the dimension of the target variable. Runtime scales exponentially with  $d$ , and so does the amount of data required for estimating the distribution, as with any multivariate density estimation task. The approach of NL-VQR allows one to exploit the structure of the domain of  $\mathbf{X}$  (via a domain-specific model like a CNN or GNN). However, exploiting the structure of  $\mathbf{Y}$  requires future work.

In conclusion, although quantile regression is a very popular tool, vector quantile regression is arguably far less known, accessible, and usable in practice due to lack of adequate tools. This is despite the fact that it is a natural extension of QR, which can be used for general statistical inference tasks. Our tool will provide the community with an off-the-shelf method performing VQR in the real world. We believe this will inspire a wide-range of applications, for which it is currently prohibitive or impossible to estimate conditional vector quantile functions.

## Acknowledgments and Disclosure of Funding

Y.R. was supported by the ISRAEL SCIENCE FOUNDATION (grant No. 729/21). Y.R. thanks Shai Feldman and Stephen Bates for discussions about vector quantile regression, and the Career Advancement Fellowship, Technion, for providing research support. A.A.R, S.V, and A.M.B were partially supported by the European Research Council (ERC) under the European Union’s Horizon 2020 research and innovation programme (grant agreement No. 863839), and by the Council For Higher Education - Planning & Budgeting Committee.

<sup>5</sup>Will be published on github upon publication.

## References

- [1] J.-D. Benamou, G. Carlier, M. Cuturi, L. Nenna, and G. Peyré. Iterative bregman projections for regularized transportation problems. *SIAM Journal on Scientific Computing*, 37(2):A1111–A1138, 2015.
- [2] N. Bonneel, M. Van De Panne, S. Paris, and W. Heidrich. Displacement interpolation using Lagrangian mass transport. *ACM Transactions on Graphics*, 30(6):Article n°158, 2011. doi: 10.1145/2070781.2024192. URL <https://hal.inria.fr/hal-00763270>.
- [3] A. Brando, J. Gimeno, J. A. Rodríguez-Serrano, and J. Vitrià. Deep non-crossing quantiles through the partial derivative. *arXiv preprint arXiv:2201.12848*, 2022.
- [4] Y. Brenier. Polar factorization and monotone rearrangement of vector-valued functions. *Communications on pure and applied mathematics*, 44(4):375–417, 1991.
- [5] G. Carlier, V. Chernozhukov, and A. Galichon. Vector quantile regression: An optimal transport approach. *Annals of Statistics*, 44(3):1165–1192, 2016. ISSN 00905364. doi: 10.1214/15-AOS1401.
- [6] G. Carlier, V. Chernozhukov, and A. Galichon. Vector quantile regression beyond the specified case. *Journal of Multivariate Analysis*, 161:96–102, 2017. ISSN 10957243. doi: 10.1016/j.jmva.2017.07.003.
- [7] G. Carlier, V. Chernozhukov, G. De Bie, and A. Galichon. Vector quantile regression and optimal transport, from theory to numerics. *Empirical Economics*, 2020. ISSN 14358921. doi: 10.1007/s00181-020-01919-y.
- [8] B. Charlier, J. Feydy, J. A. Glaunès, F.-D. Collin, and G. Durif. Kernel operations on the gpu, with autodiff, without memory overflows. *Journal of Machine Learning Research*, 22(74):1–6, 2021. URL <http://jmlr.org/papers/v22/20-275.html>.
- [9] V. Chernozhukov, I. Fernández-Val, and A. Galichon. Quantile and probability curves without crossing. *Econometrica*, 78(3):1093–1125, 2010.
- [10] V. Chernozhukov, A. Galichon, M. Hallin, and M. Henry. Monge–Kantorovich depth, quantiles, ranks and signs. *The Annals of Statistics*, 45(1):223 – 256, 2017. doi: 10.1214/16-AOS1450. URL <https://doi.org/10.1214/16-AOS1450>.
- [11] M. Cuturi. Sinkhorn distances: Lightspeed computation of optimal transport. *Advances in neural information processing systems*, 26, 2013.
- [12] S. Feldman, S. Bates, and Y. Romano. Calibrated multiple-output quantile regression with representation learning. *arXiv preprint arXiv:2110.00816*, 2021.
- [13] S. Ferradans, N. Papadakis, J. Rabin, G. Peyré, and J.-F. Aujol. Regularized discrete optimal transport. In *International Conference on Scale Space and Variational Methods in Computer Vision*, pages 428–439. Springer, 2013.
- [14] R. Flamary, N. Courty, A. Gramfort, M. Z. Alaya, A. Boisbunon, S. Chambon, L. Chapel, A. Corenflos, K. Fatras, N. Fournier, L. Gautheron, N. T. Gayraud, H. Janati, A. Rakotomamonjy, I. Redko, A. Rolet, A. Schutz, V. Seguy, D. J. Sutherland, R. Tavenard, A. Tong, and T. Vayer. Pot: Python optimal transport. *Journal of Machine Learning Research*, 22(78):1–8, 2021. URL <http://jmlr.org/papers/v22/20-451.html>.
- [15] A. Genevay, M. Cuturi, G. Peyré, and F. Bach. Stochastic optimization for large-scale optimal transport. *Advances in neural information processing systems*, 29, 2016.
- [16] R. Koenker and G. Bassett. Regression Quantiles. *Econometrica*, 46(1):33, 1978. ISSN 00129682. doi: 10.2307/1913643.
- [17] R. J. McCann. Existence and uniqueness of monotone measure-preserving maps. *Duke Mathematical Journal*, 80(2):309–323, 1995.
- [18] R. T. Rockafellar. *Conjugate duality and optimization*. SIAM, 1974.

- [19] J. Solomon, F. De Goes, G. Peyré, M. Cuturi, A. Butscher, A. Nguyen, T. Du, and L. Guibas. Convolutional wasserstein distances: Efficient optimal transportation on geometric domains. *ACM Transactions on Graphics (ToG)*, 34(4):1–11, 2015.
- [20] N. Tagasovska and D. Lopez-Paz. Single-model uncertainties for deep learning. *Advances in Neural Information Processing Systems*, 32, 2019.
- [21] C. Villani. *Topics in optimal transportation*, volume 58. American Mathematical Soc., 2021.

## A Derivations

In this section, we present the following derivations:

- Formulating one-dimensional QR as a correlation-maximization problem (Appendix A.1).
- Rephrasing correlation maximization as one-dimensional optimal transport (Appendix A.2).
- Extension of the OT-based formulation for QR to the multi-dimensional targets (Appendix A.3).
- Relaxing the dual formulation of the OT-based VQR problem (Appendix A.4).
- The equivalence between the entropic-regularized version of the OT-based primal and the relaxed dual formulation (Appendix A.5).
- Calculating the conditional (vector) quantile functions from the dual variables (Appendix A.6).

The derivations in this section are not rigorous mathematical proofs; instead they are meant to show an easy-to-follow way to obtain the high-dimensional VQR relaxed dual objective (which we eventually solve), by starting from the well-known one-dimensional QR based on the pinball loss.

### A.1 Quantile Regression as Correlation Maximization

The pinball loss defined above can be written as,

$$\begin{aligned}\rho_u(z) &= \begin{cases} uz, & z > 0 \\ (u-1)z, & z \leq 0 \end{cases} \\ &= \begin{cases} uz - z + z, & z > 0 \\ (u-1)z, & z \leq 0 \end{cases} \\ &= z^+ + (u-1)z\end{aligned}$$

where  $z^+ \triangleq \max\{0, z\}$ . Note that we also define  $z^- \triangleq \max\{0, -z\}$  which we use later. Given the continuous joint distribution  $P_{\mathbf{X}, \mathbf{Y}}$ , and assuming a linear model relates the  $u$ -th quantile of  $\mathbf{Y}$  to  $\mathbf{X}$ , then performing quantile regression involves minimizing

$$\min_{a_u, \mathbf{b}_u} \mathbb{E}_{\mathbf{X}, \mathbf{Y}} \left[ (Y - \mathbf{b}_u^\top \mathbf{X} - a_u)^+ - (1-u)(Y - \mathbf{b}_u^\top \mathbf{X} - a_u) \right]. \quad (10)$$

Define  $Z(a_u, \mathbf{b}_u) \triangleq Y - \mathbf{b}_u^\top \mathbf{X} - a_u$ , the above problem can be written as

$$\min_{a_u, \mathbf{b}_u} \mathbb{E}_{\mathbf{X}, \mathbf{Y}} \left[ Z(a_u, \mathbf{b}_u)^+ - (1-u)Z(a_u, \mathbf{b}_u) \right]. \quad (11)$$

Define  $P_u \triangleq Z(a_u, \mathbf{b}_u)^+$  and  $N_u \triangleq Z(a_u, \mathbf{b}_u)^-$  as the positive and negative deviations from the true  $u$ -th quantile, then notice that (i)  $P_u \geq 0$  and  $N_u \geq 0$ ; (ii)  $P_u - N_u = Z(a_u, \mathbf{b}_u)$ . Introducing  $P_u$  and  $N_u$  as slack variables, we can rewrite the above optimization problem as

$$\begin{aligned}\min_{a_u, \mathbf{b}_u, P_u, N_u} \quad & \mathbb{E}_{\mathbf{X}, \mathbf{Y}} [P_u - (1-u)Z(a_u, \mathbf{b}_u)] \\ \text{s.t.,} \quad & P_u \geq 0, N_u \geq 0 \\ & P_u - N_u = Z(a_u, \mathbf{b}_u), \text{ with multiplier } [V_u].\end{aligned}$$

Solving the above problem is equivalent to solving the Lagrangian formulation

$$\begin{aligned}\min_{P_u, N_u, a_u, \mathbf{b}_u} \quad & \max_{V_u} \mathbb{E}_{\mathbf{X}, \mathbf{Y}} [P_u - (1-u)Z(a_u, \mathbf{b}_u) - V_u(P_u - N_u - Z(a_u, \mathbf{b}_u))] \\ \text{s.t.,} \quad & P_u \geq 0, N_u \geq 0.\end{aligned}$$

Substituting  $Z_u(a_u, \mathbf{b}_u) = \mathbf{Y} - \mathbf{b}_u^\top \mathbf{X} - a$ , we get

$$\begin{aligned} \min_{P_u, N_u, a_u, \mathbf{b}_u} \quad & \max_{V_u} \mathbb{E}_{\mathbf{X}, \mathbf{Y}} [P_u - (1-u)(\mathbf{Y} - \mathbf{b}_u^\top \mathbf{X} - a_u) - V_u (P_u - N_u - \mathbf{Y} + \mathbf{b}_u^\top \mathbf{X} + a_u)] \\ \text{s.t.,} \\ P_u \geq 0, N_u \geq 0. \end{aligned}$$

In the first term,  $\mathbf{Y}$  can be omitted because it is independent of the optimization variables, and in the second term,  $\mathbf{Y}$  can be separated, this yields

$$\begin{aligned} \max_{V_u} \mathbb{E}_{\mathbf{X}, \mathbf{Y}} [V_u \mathbf{Y}] + \min_{P_u, N_u, a_u, \mathbf{b}_u} \mathbb{E}_{\mathbf{X}, \mathbf{Y}} [P_u - (u-1)(\mathbf{b}_u^\top \mathbf{X} + a_u) - V_u (P_u - N_u + \mathbf{b}_u^\top \mathbf{X} + a_u)] \\ \text{s.t.,} \\ P_u \geq 0, N_u \geq 0. \end{aligned}$$

Rewriting the terms by separating  $a_u, \mathbf{b}_u, P_u, N_u$  yields

$$\begin{aligned} \max_{V_u} \mathbb{E}_{\mathbf{X}, \mathbf{Y}} [V_u \mathbf{Y}] + \min_{P_u, N_u, a_u, \mathbf{b}_u} \mathbb{E}_{\mathbf{X}, \mathbf{Y}} [P_u (1 - V_u) + N_u V_u - a_u (V_u - (1-u)) - \mathbf{b}_u^\top (V_u \mathbf{X} - (1-u) \mathbf{X})] \\ \text{s.t.,} \\ P_u \geq 0, N_u \geq 0. \end{aligned}$$

By treating  $P_u, N_u, a_u, \mathbf{b}_u$  as Lagrange multipliers we can obtain the dual formulation. Since  $P_u, N_u \geq 0$ , they must participate in inequality constraints, and since  $a_u, \mathbf{b}_u$  are unconstrained, they participate in equality constraints. Thus,

$$\begin{aligned} \max_{V_u} \mathbb{E}_{\mathbf{X}, \mathbf{Y}} [V_u Y_u] \\ \text{s.t. } V_u \geq 0 & \quad [N_u] \\ V_u \leq 1 & \quad [P_u] \\ \mathbb{E}_{\mathbf{X}, \mathbf{Y}} [V_u] = (1-u) & \quad [a_u] \\ \mathbb{E}_{\mathbf{X}, \mathbf{Y}} [V_u \mathbf{X}] = (1-u) \mathbb{E} [\mathbf{X}] & \quad [\mathbf{b}_u]. \end{aligned}$$

Note that (i) complementary slackness dictates that we always have  $P_u, N_u \geq 0$ , and that (ii) the last two constraints can be seen together as implying the mean independence condition of  $\mathbb{E} [\mathbf{X}|V] = \mathbb{E} [\mathbf{X}]$ .

Solving for multiple quantiles simultaneously can be achieved by minimizing the sum of above optimization problem  $\forall u \in [0, 1]$ . In addition we demand monotonicity of the estimated quantiles, such that  $u \geq u' \implies \mathbf{b}_u^\top \mathbf{X} + a_u \geq \mathbf{b}_{u'}^\top \mathbf{X} + a_{u'}$ . According to the KKT conditions, the solution to the above problem must satisfy complementary slackness, which in this case means

$$\begin{aligned} (1 - V_u) P_u &= 0 \\ V_u N_u &= 0. \end{aligned}$$

Following the definitions of  $P_u, N_u$ , we have the following relation between the estimate quantile  $\mathbf{b}_u^\top \mathbf{X} + a_u$  and  $V_u$ :

$$\begin{cases} \mathbf{Y} > \mathbf{b}_u^\top \mathbf{X} + a_u \implies P_u > 0 & \implies V_u = 1 \\ \mathbf{Y} < \mathbf{b}_u^\top \mathbf{X} + a_u \implies N_u > 0 & \implies V_u = 0 \\ \mathbf{Y} = \mathbf{b}_u^\top \mathbf{X} + a_u \implies P_u = N_u = 0 & \implies 0 \leq V_u \leq 1 \end{cases}$$

Since  $P_{\mathbf{X}, \mathbf{Y}}$  is a continuous distribution, then for any  $a_u, \mathbf{b}_u$ , we have  $\mathbb{P} [\mathbf{Y} = \mathbf{b}_u^\top \mathbf{X} + a_u] = 0$ . Thus in practice we can ignore this case and write

$$V_u = \mathbb{I} \{ \mathbf{Y} \geq \mathbf{b}_u^\top \mathbf{X} + a_u \}. \quad (12)$$

Therefore the monotonicity constraint translates to  $V_u$  as

$$u \geq u' \implies \mathbf{b}_u^\top \mathbf{X} + a_u \geq \mathbf{b}_{u'}^\top \mathbf{X} + a_{u'} \implies V_u \leq V_{u'}.$$

Adding the monotonicity constraint on  $V_u$  to the gives rise to a new dual problem:

$$\begin{aligned}
\max_{V_u} \quad & \int_0^1 \mathbb{E}_{\mathbf{X}, \mathbf{Y}} [V_u Y_u] du \\
\text{s.t.} \quad & V_u \geq 0 \quad [N_u] \\
& V_u \leq 1 \quad [P_u] \\
& \mathbb{E}_{\mathbf{X}, \mathbf{Y}} [V_u] = (1 - u) \quad [a_u] \\
& \mathbb{E}_{\mathbf{X}, \mathbf{Y}} [V_u \mathbf{X}] = (1 - u) \mathbb{E} [\mathbf{X}] \quad [\mathbf{b}_u] \\
& u \geq u' \implies V_u \leq V_{u'}.
\end{aligned}$$

Let us now consider a dataset  $\{(\mathbf{x}_i, y_i)\}_{i=1}^N$  of i.i.d. samples from  $P_{\mathbf{X}, \mathbf{Y}}$  where  $\mathbf{x}_i \in \mathbb{R}^k$  and  $y_i \in \mathbb{R}$ . We are interested in calculating  $T$  quantiles for levels  $u_1 = 0 < u_2 < \dots < u_T \leq 1$ . Furthermore, denote the sample mean  $\bar{\mathbf{x}} \in \mathbb{R}^k$  where  $\bar{\mathbf{x}}_k = \sum_{i=1}^N x_{i,k}/N$ . By discretizing the above problem, we arrive at

$$\begin{aligned}
\max_{V_{\tau, i}} \quad & \sum_{\tau=1}^T \sum_{i=1}^N V_{\tau, i} y_i \\
\text{s.t.} \quad & V_{\tau, i} \geq 0 \quad [N_{\tau, i}] \\
& V_{\tau, i} \leq 1 \quad [P_{\tau, i}] \\
& \frac{1}{N} \sum_{i=1}^N V_{\tau, i} = (1 - u_{\tau}) \quad [a_{\tau}] \\
& \frac{1}{N} \sum_{i=1}^N V_{\tau, i} x_{i,k} = (1 - u_{\tau}) \bar{x}_k \quad [b_{\tau, k}] \\
& V_{T, i} \leq V_{T-1, i} \leq \dots \leq V_{1, i}.
\end{aligned}$$

Now we can vectorize the above formulation by defining the matrix  $\mathbf{V} \in \mathbb{R}^{T \times N}$  containing elements  $V_{\tau, i}$ , the first-order finite differences matrix

$$\mathbf{D} = \begin{pmatrix} 1 & 0 & \cdots & 0 \\ -1 & 1 & & 0 \\ 0 & -1 & & \vdots \\ 0 & 0 & & \\ \vdots & \vdots & & 1 & 0 \\ 0 & \cdots & & -1 & 1 \end{pmatrix} \in \mathbb{R}^{T \times T},$$

and the vector of desired quantile levels,  $\mathbf{u} = [u_1, \dots, u_T]^\top$ . The monotonicity constraint therefore becomes  $\mathbf{v}_i^\top \mathbf{D} \geq 0 \forall i = 1, \dots, N$  where  $\mathbf{v}_i$  is the  $i$ -th column of  $\mathbf{V}$ . We also denote the covariates matrix  $\mathbf{X} \in \mathbb{R}^{N \times k}$  and response vector  $\mathbf{y} \in \mathbb{R}^N$ . Thus, the problem vectorizes as,

$$\begin{aligned}
\max_{\mathbf{V}} \quad & \mathbf{1}_T^\top \mathbf{V} \mathbf{y} \\
\text{s.t.} \quad & V_{\tau, i} \geq 0 \quad [N_{\tau, i}] \\
& V_{\tau, i} \leq 1 \quad [P_{\tau, i}] \\
& \frac{1}{N} \mathbf{V} \mathbf{1}_N = (\mathbf{1}_T - \mathbf{u}) \quad [\mathbf{a}] \\
& \frac{1}{N} \mathbf{V} \mathbf{X} = (\mathbf{1}_T - \mathbf{u}) \bar{\mathbf{x}}^\top \quad [\mathbf{B}] \\
& \mathbf{V}^\top \mathbf{D} \geq 0.
\end{aligned}$$

where  $\mathbf{a} \in \mathbb{R}^T$  and  $\mathbf{B} \in \mathbb{R}^{T \times k}$  are the dual variables which contain the regression coefficients per quantile level. We can observe the following for the above problem:

1. For any random variable, its zeroth quantile is smaller than or equal to any values the variable takes. In particular, for  $\tau = 0$  we have  $V_{0,i} = 1 \forall i$  because from eq. (12) we know that  $V_{0,i}$  is the indicator that  $y_i$  is greater than the zeroth quantile of  $Y$ .
2. The last constraint  $\mathbf{V}^\top \mathbf{D} \geq 0$ , which enforces non-increasing monotonicity along the quantile level, i.e.,  $V_{\tau,i} \leq V_{\tau',i} \forall \tau \geq \tau'$ , also enforces that  $V_{T,i} \geq 0$ .

Therefore, we can observe that the first ( $V_{\tau,i} \geq 0$ ), second ( $V_{\tau,i} \leq 1$ ) and last ( $\mathbf{V}^\top \mathbf{D} \geq 0$ ) constraints are partially-redundant and can be condensed into only two vectorized constraints: (1)  $\mathbf{V}^\top \mathbf{D} \geq 0$  which ensures monotonicity and non-negativity of all elements in  $\mathbf{V}$ ; (2)  $\mathbf{V}^\top \mathbf{D} \mathbf{1}_T \leq \mathbf{1}_N$  which enforces that  $V_{0,i} \leq 1 \forall i$ . Notice that condensing the constraints in this manner comes with the inability to interpret the meaning of the Lagrange multipliers  $P_{\tau,i}, N_{\tau,i}$ . However, the advantage is that we have less constraints in total and the interpretability of the multipliers  $\mathbf{a}, \mathbf{B}$  is maintained. Thus, we arrive at the following vectorized problem,

$$\begin{aligned} & \max_{\mathbf{V}} \mathbf{1}_T^\top \mathbf{V} \mathbf{y} \\ \text{s.t. } & \frac{1}{N} \mathbf{V} \mathbf{1}_N = (\mathbf{1}_T - \mathbf{u}) & [\mathbf{a}] \\ & \frac{1}{N} \mathbf{V} \mathbf{X} = (\mathbf{1}_T - \mathbf{u}) \bar{\mathbf{x}}^\top & [\mathbf{B}] \\ & \mathbf{V}^\top \mathbf{D} \geq 0 \\ & \mathbf{V}^\top \mathbf{D} \mathbf{1}_T \leq \mathbf{1}_N. \end{aligned}$$

## A.2 Correlation Maximization as Optimal Transport

Following Carlier et al. [5], the above problem can be re-formulated as an Optimal Transport problem, i.e. the problem of finding a mapping between two probability distributions.

Assume we are now interested in estimating the quantiles of  $Y$  at  $T$  uniformly-sampled levels,  $[u_1, \dots, u_T]^\top = [\frac{1}{T}, \frac{2}{T}, \dots, \frac{T}{T}]^\top$ . In the above problem, one can decompose the objective as

$$\mathbf{1}_T^\top \mathbf{V} \mathbf{y} = (\mathbf{1}_T^\top \mathbf{D}^{-\top}) (\mathbf{D}^\top \mathbf{V}) \mathbf{y} = (\mathbf{D}^{-1} \mathbf{1}_T)^\top (\mathbf{D}^\top \mathbf{V}) \mathbf{y}.$$

If we then denote

$$\begin{aligned} \mathbf{\Pi} &= \frac{1}{N} \mathbf{D}^\top \mathbf{V} \in \mathbb{R}^{T \times N} \\ \mathbf{u} &= \frac{1}{T} \mathbf{D}^{-1} \mathbf{1}_T = \left[ \frac{1}{T}, \frac{2}{T}, \dots, \frac{T}{T} \right]^\top \in \mathbb{R}^T, \end{aligned}$$

then we can write the objective as  $NT \cdot \mathbf{u}^\top \mathbf{\Pi} \mathbf{y}$ . In addition, denote

$$\begin{aligned} \boldsymbol{\mu} &= \mathbf{D}^\top (\mathbf{1}_T - \mathbf{u}) = \frac{1}{T} \mathbf{1}_T \in \mathbb{R}^T \\ \boldsymbol{\nu} &= \frac{1}{N} \mathbf{1}_N \in \mathbb{R}^N, \end{aligned}$$

which represent (respectively) the empirical probability measure of the quantile levels  $\mathbf{u}$  and the data points  $(\mathbf{X}, \mathbf{y})$  (we choose both measures to be uniform). Now, by using the decomposed objective, and by multiplying the first two constraints by  $\mathbf{D}^\top$  on either side, we obtain the following equivalent problem:

$$\begin{aligned} & \max_{\mathbf{\Pi} \geq 0} \mathbf{u}^\top \mathbf{\Pi} \mathbf{y} \\ \text{s.t. } & \mathbf{\Pi} \mathbf{1}_N = \boldsymbol{\mu} = \frac{1}{T} \mathbf{1}_T & [\mathbf{D}^{-\top} \mathbf{a}] \\ & \mathbf{\Pi} \mathbf{X} = \boldsymbol{\mu} \boldsymbol{\nu}^\top \mathbf{X} = \frac{1}{T} \mathbf{1}_T \bar{\mathbf{x}}^\top & [\mathbf{D}^{-\top} \mathbf{B}] \\ & \mathbf{1}_T^\top \mathbf{\Pi} \leq \boldsymbol{\nu} = \frac{1}{N} \mathbf{1}_N^\top. & \end{aligned} \tag{13}$$

Note that (i) we ignore the normalization constants where they do not affect the solution; (ii) the Lagrange multipliers are scaled by  $\mathbf{D}^{-\top}$  since the constraints are scaled by  $\mathbf{D}^\top$ .

The interpretation of this formulation is that we seek a mapping  $\Pi$  between the distribution of the quantile levels  $\mathbf{u}$  and the distribution of the data points  $\mathbf{Y}|\mathbf{X}$ , subject to constraints on the map which ensure that the marginal distributions of this map are the empirical measures  $\mu$  and  $\nu$ , and that mean independence  $\mathbb{E}[\mathbf{X}|\mathbf{U}] = \mathbb{E}[\mathbf{X}]$  holds. Each individual entry  $\Pi_{\tau,i}$  in this map is the probability mass attached to  $(u_\tau, \mathbf{x}_i, y_i)$  in this optimal joint distribution.

### A.3 Extending the Optimal Transport Formulation to Vector Quantiles

We now wish to deal with the case where the target variable can be a vector. Observe that for the scalar case, we can write the OT objective as

$$\mathbf{u}^\top \Pi \mathbf{y} = \sum_{\tau=1}^T \sum_{i=1}^N \Pi_{\tau,i} u_\tau y_i = \Pi \odot \mathbf{S},$$

where  $\mathbf{S} \in \mathbb{R}^{T \times N}$  is a matrix of pairwise products, i.e.  $S_{\tau,i} = u_\tau y_i$ , and  $\odot$  denotes the Hadamard (elementwise) product.

Now let us assume that  $\mathbf{y}_i \in \mathbb{R}^d$  for any  $d \geq 1$ , and thus our target data will now be arranged as  $\mathbf{Y} \in \mathbb{R}^{N \times d}$ . Moreover, the quantile levels must now also  $d$ -dimensional, since we have a quantile level dimension for each data dimension. We will choose a uniform grid on  $[0, 1]^d$  on which to compute our vector quantiles. Along each dimension of this grid we sample  $T$  equally-spaced points, giving us in total  $T^d$  points in  $d$  dimensions.

To keep the formulation of the optimization problem two dimensional, we arrange the coordinates of these points as the matrix  $\mathbf{U} \in \mathbb{R}^{T^d \times d}$ . Thus, we can naturally extend the pairwise product matrix  $\mathbf{S}$  to the multi-dimensional case using a  $d$ -dimensional inner-product between each point on the quantile level grid  $\mathbf{U}$  and each target point in  $\mathbf{Y}$ . This yields the simple form  $\mathbf{S} = \mathbf{U} \mathbf{Y}^\top$ , where  $\mathbf{S} \in \mathbb{R}^{T^d \times N}$ , which can be plugged in to the above formulation (13) and solved directly. By also setting  $\bar{\mathbf{x}} = \mathbf{0}$  we obtain eq. (5).

### A.4 Relaxing the Exact Optimal Transport Dual Formulation

Recall the exact dual formulation of the OT-based primal VQR problem (5):

$$\begin{aligned} \min_{\psi, \varphi, \beta} \quad & \sum_{j=1}^N \psi_j \nu_j + \sum_{i=1}^{T^d} \varphi_i \mu_i \\ \text{s.t. } \forall i, j : \quad & \varphi_i + \beta_i^\top \mathbf{x}_j + \psi_j \geq \mathbf{u}_i^\top \mathbf{y}_j \end{aligned}$$

The above problem has a unique solution [5]. Thus, first-order optimality conditions for each  $\varphi_i$  yield

$$\varphi_i = \max_j \{ \mathbf{u}_i^\top \mathbf{y}_j - \beta_i^\top \mathbf{x}_j - \psi_j \}.$$

Substituting the optimal  $\varphi_i$  into the dual formulation results in an unconstrained but exact min-max problem:

$$\min_{\psi, \beta} \sum_{j=1}^N \psi_j \nu_j + \sum_{i=1}^{T^d} \mu_i \max_j \{ \mathbf{u}_i^\top \mathbf{y}_j - \beta_i^\top \mathbf{x}_j - \psi_j \}. \quad (14)$$

We can relax this problem by using a smooth approximation for the max operator, given by

$$\max_j(\mathbf{x}) \approx \varepsilon \log \left( \sum_j \exp \left( \frac{x_j}{\varepsilon} \right) \right).$$

Plugging the smooth approximation into eq. (14) yields the relaxed dual in eq. (7).

### A.5 Equivalence between Regularized Primal and Relaxed Dual

Adding an entropic regularization term to the OT-based primal formulation of the VQR problem (5), and converting into a minimization problem yields,

$$\begin{aligned} \min_{\Pi} \quad & \langle \Pi, -\mathbf{S} \rangle + \varepsilon \langle \Pi, \log \Pi \rangle \\ \text{s.t. } \quad & \Pi^\top \mathbf{1}_{T^d} = \nu \quad [-\psi] \\ & \Pi \mathbf{1}_N = \mu \quad [-\varphi] \\ & \Pi \mathbf{X} = \mathbf{0} \quad [-\beta]. \end{aligned} \quad (15)$$

Note that the entropic regularization term can be interpreted as minimization of the KL-divergence between the joint distribution  $\Pi$  and the product of marginals, i.e.,  $\mathcal{D}_{\text{KL}}(\Pi \parallel \mu\nu^\top)$ .

In order to show the equivalence between this regularized problem and the relaxed dual (7), the key idea is to use the Fenchel-Rockafeller duality theorem [18]. This provides a convenient way to write the dual of an optimization problem in terms of the convex conjugate functions of its objective.

In order to apply this approach, we reformulate eq. (15) into an unconstrained problem of the following form:

$$\min_{\mathbf{W} \in \mathcal{W}} f^*(\mathcal{A}^* \mathbf{W}) + g^*(\mathbf{W}) = \max_{\mathbf{V} \in \mathcal{V}} -f(-\mathbf{V}) - g(\mathcal{A}\mathbf{V}),$$

where we define a pair of operators  $\mathcal{A} : \mathcal{V} \mapsto \mathcal{W}$  and  $\mathcal{A}^* : \mathcal{W}^* \mapsto \mathcal{V}^*$  adjoint to each other;  $f : \mathcal{V} \mapsto \mathbb{R}$ ,  $f^* : \mathcal{V}^* \mapsto \mathbb{R}$  and  $g : \mathcal{W} \mapsto \mathbb{R}$ ,  $g^* : \mathcal{W}^* \mapsto \mathbb{R}$  are pairs of convex conjugate functions. In our problem  $\mathcal{W} = \mathcal{W}^*$  and  $\mathcal{V} = \mathcal{V}^*$  are the vector spaces  $\mathcal{W} = \mathcal{W}^* = \mathbb{R}^{T^d \times N}$  and  $\mathcal{V} = \mathcal{V}^* = \mathbb{R}^{T^d} \times \mathbb{R}^N \times \mathbb{R}^{T^d \times k}$ . Furthermore, we define the operator

$$\mathcal{A}^* \Pi = (\Pi^\top \mathbf{1}_{T^d}, \Pi \mathbf{1}_N, \Pi \mathbf{X})$$

and an indicator function,

$$i_{\mathbf{a}}(\mathbf{z}) = \begin{cases} 0, & \mathbf{z} = \mathbf{a}, \\ \infty, & \mathbf{z} \neq \mathbf{a}. \end{cases}$$

We can now represent eq. (15) as an unconstrained problem,

$$\min_{\Pi} \langle \Pi, -\mathbf{S} \rangle + \varepsilon \langle \Pi, \log \Pi \rangle + i_{(\nu, \mu, \mathbf{0})}(\mathcal{A}^* \Pi) \quad (16)$$

To derive the adjoint operator of  $\mathcal{A}^*$  we can write,

$$\begin{aligned} \langle (\psi, \varphi, \beta), \mathcal{A}^* \Pi \rangle_{\mathcal{V}} &= \langle \psi, \Pi^\top \mathbf{1}_{T^d} \rangle + \langle \varphi, \Pi \mathbf{1}_N \rangle + \langle \beta, \Pi \mathbf{X} \rangle \\ &= \text{tr}(\psi^\top \Pi^\top \mathbf{1}_{T^d}) + \text{tr}(\varphi^\top \Pi \mathbf{1}_N) + \text{tr}(\beta^\top \Pi \mathbf{X}) \\ &= \langle \mathbf{1}_{T^d} \psi^\top, \Pi \rangle + \langle \varphi \mathbf{1}_N^\top, \Pi \rangle + \langle \beta \mathbf{X}^\top, \Pi \rangle \\ &= \langle \mathcal{A}(\psi, \varphi, \beta), \Pi \rangle_{\mathcal{W}}. \end{aligned}$$

Thus,  $\mathcal{A}(\psi, \varphi, \beta) = \mathbf{1}_{T^d} \psi^\top + \varphi \mathbf{1}_N^\top + \beta \mathbf{X}^\top$ .

We define the functions

$$\begin{aligned} f^*(\mathcal{A}^* \Pi) &= i_{(\nu, \mu, \mathbf{0})}(\mathcal{A}^* \Pi) \\ g^*(\Pi) &= \langle \Pi, -\mathbf{S} \rangle + \varepsilon \langle \Pi, \log \Pi \rangle, \end{aligned}$$

and their corresponding convex conjugates,

$$\begin{aligned} f(\psi, \varphi, \beta) &= \langle (\psi, \varphi, \beta), (\nu, \mu, \mathbf{0}) \rangle_{\mathcal{V}} = \langle \psi, \nu \rangle + \langle \varphi, \mu \rangle \\ g(\mathbf{W}) &= \varepsilon \sum_{ij} \exp\left(\frac{W_{ij} + S_{ij} - 1}{\varepsilon}\right). \end{aligned}$$

Using  $f^*$  and  $g^*$ , we can write (16) as  $\min_{\mathbf{W}} \{f^*(\mathcal{A}^* \mathbf{W}) + g^*(\mathbf{W})\}$ , then by the Fenchel-Rockafeller duality theorem, we get the equivalent dual form  $\max_{\mathbf{V}} \{-f(-\mathbf{V}) - g(\mathcal{A}\mathbf{V})\}$ . Substituting  $\mathbf{V} = (-\psi, -\varphi, -\beta)$ , converting to a minimization problem, and omitting constant factors in the objective, we get

$$\min_{\psi, \varphi, \beta} \psi^\top \nu + \varphi^\top \mu + \varepsilon \sum_{i=1}^{T^d} \sum_{j=1}^N \exp\left(\frac{1}{\varepsilon} (S_{ij} - \psi_j - \varphi_i - \beta_i^\top \mathbf{x}_j)\right). \quad (17)$$

Now we write  $\varphi$  in terms of  $\psi, \beta$  by using a first-order optimality condition of the above problem w.r.t.  $\varphi_i$ :

$$0 = \mu_i - \varepsilon \sum_j \exp \left( \frac{1}{\varepsilon} (S_{ij} - \psi_j - \varphi_i - \beta_i^\top \mathbf{x}_j) \right) \quad (18)$$

$$\exp \left( \frac{\varphi_i}{\varepsilon} \right) = \frac{\varepsilon}{\mu_i} \sum_j \exp \left( \frac{1}{\varepsilon} (S_{ij} - \psi_j - \beta_i^\top \mathbf{x}_j) \right) \quad (19)$$

$$\varphi_i = \varepsilon \log \left( \frac{\varepsilon}{\mu_i} \sum_j \exp \left( \frac{1}{\varepsilon} (S_{ij} - \psi_j - \beta_i^\top \mathbf{x}_j) \right) \right) \quad (20)$$

Finally, substituting eqs. (19) and (20) into eq. (17) and omitting constant terms yields,

$$\min_{\psi, \beta} \sum_{j=1}^N \psi_j \nu_j + \varepsilon \sum_{i=1}^{T^d} \mu_i \log \left( \sum_{j=1}^N \exp \left( \frac{1}{\varepsilon} (S_{ij} - \beta_i^\top \mathbf{x}_j - \psi_j) \right) \right), \quad (21)$$

where  $S_{ij} = \mathbf{u}_i^\top \mathbf{y}_j$ . Thus, we obtain that eq. (21) is equal to eq. (7).

In summary, we have shown that the relaxed dual formulation of the VQR problem that we solve (7), is equivalent to an entropic-regularized version of the OT-based primal formulation eq. (5).

## A.6 Extracting the Vector Quantile Regression Coefficients

The dual variables obtained from the OT formulation are  $\varphi \in \mathbb{R}^{T^d}$  and  $\beta \in \mathbb{R}^{T^d \times k}$ . In the case of scalar quantiles ( $d = 1$ ) we can obtain the conditional quantile function from the dual variables by applying  $\mathbf{D}^\top$  (see eq. (13)<sup>6</sup>). Then,  $Q_{\mathbf{Y}|\mathbf{X}}(\mathbf{u}; \mathbf{x}) = [\mathbf{D}^\top (\beta \mathbf{x} + \varphi)]_{\mathbf{u}}$ . Notice that this is effectively taking the first-order discrete derivative. As shown in Carlier et al. [7], based on Brenier's theorem [4] the quantile function is a Brenier map between the probability measures of  $\mathbf{U}$  and  $\mathbf{Y}$ . Thus, the quantile function is the gradient of a convex function, which can be written as  $Q_{\mathbf{Y}|\mathbf{X}}(\mathbf{u}'; \mathbf{x}) = \nabla_{\mathbf{u}} \phi(\mathbf{u}', \mathbf{x})$  where  $\phi(\mathbf{u}, \mathbf{x}) = \beta_{\mathbf{u}}^\top \mathbf{x} + \varphi_{\mathbf{u}}$  is convex in  $\mathbf{u}$ .

In the vector case, we have  $T^d$  discrete  $d$ -dimensional quantile levels. Equivalently, the relation between the dual variables and the quantile function is then  $Q_{\mathbf{Y}|\mathbf{X}}(\mathbf{u}'; \mathbf{x}) = [\nabla_{\mathbf{u}} \{\beta \mathbf{x} + \varphi\}]_{\mathbf{u}'}$ . Notice that  $\beta \mathbf{x} + \varphi \in \mathbb{R}^{T^d}$  and its gradient with respect to  $\mathbf{u}$ ,  $\nabla_{\mathbf{u}} \{\beta \mathbf{x} + \varphi\}$ , is in  $\mathbb{R}^{T^d \times d}$ . We then evaluate its gradient at a point  $\mathbf{u}'$  to obtain the  $d$ -dimensional quantile.

## B Intuitions About Vector Quantile Functions

To interpret the meaning of vector quantile functions, let us consider the 2-dimensional case, where we assume  $\mathbf{Y} = (Y_1, Y_2)^\top$ . Given a specific covariates vector  $\mathbf{x} = (x_1, \dots, x_k)^\top$ , and level  $\mathbf{u} = (u_1, u_2)^\top$  we may write the components of the conditional vector quantile function as,

$$Q_{\mathbf{Y}|\mathbf{X}}(\mathbf{u}; \mathbf{x}) = \begin{bmatrix} Q_1(\mathbf{u}; \mathbf{x}) \\ Q_2(\mathbf{u}; \mathbf{x}) \end{bmatrix} = \begin{bmatrix} Q_{Y_1|Y_2, \mathbf{X}}(u_1; Q_{Y_2|\mathbf{X}}(u_2; \mathbf{x}), \mathbf{x}) \\ Q_{Y_2|Y_1, \mathbf{X}}(u_2; Q_{Y_1|\mathbf{X}}(u_1; \mathbf{x}), \mathbf{x}) \end{bmatrix},$$

where  $Q_{Y_i|Y_j, \mathbf{X}}(u; y, \mathbf{x})$  denotes the scalar quantile function of the random variable  $Y_i$  at level  $u$ , given  $Y_j = y, \mathbf{X} = \mathbf{x}$ . Thus, for example, the first component  $Q_1(\mathbf{u}; \mathbf{x})$  is a 2D surface where moving along  $u_1$  for a fixed  $u_2$  yields a scalar, non-decreasing function representing the quantiles of  $Y_1$  when  $Y_2$  is at a value corresponding to level  $u_2$  (see Figure 5b). In addition, the vector quantile function is co-monotonic with  $\mathbf{u}$  in the sense defined by eq. (1). For higher dimensions, it becomes more involved as the conditioning in each component is on the vector quantile of all the remaining components of the target  $\mathbf{Y}$  (Figure 5c).

Another interesting property of VQFs is that they allow a natural extension of  $\alpha$ -confidence intervals to high dimensional distributions (Figure 1a). Consider the 2d case. By fixing e.g.  $u_1$  to be one of  $\{\alpha, 1 - \alpha\}$  and then sweeping over  $u_2$  (and vice versa), on each of the quantile component surfaces  $Q_1(\mathbf{u}), Q_2(\mathbf{u})$  we obtain a contour on each surface (Figure 1a, left and right). Mapping this contour

<sup>6</sup>where  $\varphi = \mathbf{D}^{-\top} \mathbf{a}$  and  $\beta = \mathbf{D}^{-\top} \mathbf{B}$ .

back to the domain of  $\mathbf{Y}$  by using the values of  $Q_1(\mathbf{u}), Q_2(\mathbf{u})$  along it, we obtain a contour of arbitrary shape, which contains  $100 \cdot (1 - 2\alpha)^d$  percent of the  $d$ -dimensional distribution (Figure 1a, middle). In contrast, if one were to estimate  $d$  one-dimensional  $\alpha$ -confidence intervals separately for each component of  $\mathbf{Y}$  the shape of the resulting contour will always be box-shaped.

## C Experiments

### C.1 Synthetic Datasets

Below we describe the four synthetic datasets which were used in the experiments.

**MVN.** Data was generated from a linear model  $\mathbf{y} = \mathbf{Ax} + \boldsymbol{\eta}$ , where  $\mathbf{x} \sim \mathbb{U}[0, 1]^k$ ,  $\mathbf{A} \in \mathbb{R}^{d \times k}$  is a random projection matrix and  $\boldsymbol{\eta}$  is multivariate Gaussian noise with a random covariance matrix.

**Conditional-banana.** This dataset was introduced by Feldman et al. [12], and inspired by a similar dataset in Carlier et al. [6]. The target variable  $\mathbf{Y} \in \mathbb{R}^2$  has a banana-shaped conditional distribution, and its shape changes non-trivially when conditioned on a continuous-valued covariate  $\mathbf{X} \in \mathbb{R}$  (see the left-most column of the panel presented in Figure 10). The data generating process is defined as follows

$$\begin{aligned} \mathbf{X} &\sim \mathbb{U}[0.8, 3.2], \quad \mathbf{z} \sim \mathbb{U}[-\pi, \pi], \quad \phi \sim \mathbb{U}[0, 2\pi], \quad \mathbf{r} \sim \mathbb{U}[-0.1, 0.1] \\ \hat{\boldsymbol{\beta}} &\sim \mathbb{U}[0, 1]^k, \quad \boldsymbol{\beta} = \frac{\hat{\boldsymbol{\beta}}}{\|\hat{\boldsymbol{\beta}}\|_1} \\ \mathbf{y}_0 &= \frac{1}{2}(-\cos(\mathbf{Z}) + 1) + \mathbf{r} \sin(\phi) + \sin(\mathbf{X}), \quad \mathbf{y}_1 = \frac{\mathbf{Z}}{\boldsymbol{\beta} \mathbf{X}} + \mathbf{r} \cos(\phi), \end{aligned}$$

and then  $\mathbf{Y} = [\mathbf{y}_0, \mathbf{y}_1]^\top$ .

**Synthetic glasses.** This dataset was introduced by Brando et al. [3]. The target variable  $\mathbf{Y} \in \mathbb{R}$  has a bimodal conditional distribution. The mode locations shift periodically when conditioned on a continuous-valued covariate  $\mathbf{X} \sim \mathbb{U}[0, 1]$  (see Figure 9a). The data generating process is defined as

$$\begin{aligned} 0 < z_1 < 3\pi, \quad \pi < z_2 < 4\pi, \quad \epsilon &\sim \text{Beta}(\alpha = 0.5, \beta = 1), \quad \gamma \sim \text{Categorical}(0, 1) \\ \mathbf{y}_1 &= 5 \sin(z_1) + 2.5 + \epsilon, \quad \mathbf{y}_2 = 5 \sin(z_2) + 2.5 - \epsilon \\ \mathbf{y} &= \gamma \mathbf{y}_1 + (1 - \gamma) \mathbf{y}_2. \end{aligned}$$

**Rotating star.** In this dataset, the target variable of  $\mathbf{Y} \in \mathbb{R}^2$  has a star-shaped conditional distribution, and its shape is rotated by  $\mathbf{X} \in \mathbb{R}$  degrees when conditioned on a discrete-valued  $\mathbf{X}$ , taking values in  $[0, 10, 20, \dots, 60]$ . Data is generated based on a  $600 \times 600$  binary image of a star. See the first column in Figure 11 to visualize conditional distributions as a function of  $\mathbf{X}$ . Since conditional distributions differ only by a rotation,  $\mathbb{E}[\mathbf{Y}|\mathbf{X}]$  remains the same for all  $\mathbf{X}$ . However, the shape of the distribution changes substantially with  $\mathbf{X}$ , especially in tails. Thus, this dataset is a challenging candidate for estimating vector quantiles which must also represent these tails in order to properly recover the shape of the conditional distribution.

### C.2 Evaluation Metrics

The quality of an estimated CVQF can be measured by how well it upholds strong representation and co-monotonicity (eqs. (1) and (2)). However, measuring strong representation requires knowledge of the ground-truth joint distribution  $P_{(\mathbf{X}, \mathbf{Y})}$  or its conditional quantile function. With synthetic data, adherence to strong representation can be measured via several proxy metrics. The second key property, violations of co-monotonicity, can be measured directly. Below we describe the metrics we use to evaluate these properties on estimated conditional quantile functions.

**Entropy of inverse CVQF.** If strong representation holds, the inverted CVQF,  $\hat{Q}_{\mathbf{Y}|\mathbf{X}}^{-1}(\mathbf{Y}|\mathbf{X})$ , must result in a uniform distribution, when evaluated on samples drawn from the true conditional distribution. As a measure of uniformity, we calculate a normalized entropy of the inverted CVQF. The inversion procedure is done as follows.

1. Sample  $L$  evaluation covariate vectors,  $\{\mathbf{x}_l\}_{l=1}^L$  values at random from the ground truth distribution  $P_{\mathbf{X}}$ .
2. For each  $\mathbf{x}_l$ ,

- (a) Sample  $M$  points  $\{\mathbf{y}_{m,l}\}_{m=1}^M$  from  $\mathbf{Y}|\mathbf{X} = \mathbf{x}_l$ .
- (b) For each  $\mathbf{y}_{m,l}$ , find the level of the closest vector quantile w.r.t. the Euclidean distance, i.e.
$$\mathbf{u}_{m,l} = \arg \min_{\mathbf{u}'} \left\| \mathbf{y}_m - \hat{Q}_{\mathbf{Y}|\mathbf{X}}(\mathbf{u}'; \mathbf{x}_l) \right\|_2.$$
- (c) For  $i \in \{1, \dots, T^d\}$  denote  $c_i$  as the number of times that the quantile level  $i$  is found in  $\{\mathbf{u}_{m,l}\}_{m=1}^M$ , and calculate  $p_i = c_i/M$ .
- (d) Calculate the entropy  $h_l = -\sum_i p_i \log p_i$  and the normalized entropy  $\tilde{h}_l = (\exp(h_l) - 1) / (T^d - 1)$ .
3. Report the CVQF inverse entropy as  $\frac{1}{L} \sum_l \tilde{h}_l$ .

Note that,

1. The entropy metric is normalized such that its values are in  $[0, 1]$  where 1 corresponds to a uniform distribution, and 0 corresponds to a delta distribution.
2. Some non-uniformity arises due to the quantization of the quantile level grid into  $T$  discrete levels per dimension. We report a reference entropy, calculated on a uniform sample of  $M$  quantile-level grid points.
3. We used  $L = 20$  and  $M = 4000$ .

**Distribution distance (KDE-L1).** Since the CVQF fully represents the conditional distribution  $P_{(\mathbf{Y}|\mathbf{X})}$  it can serve as a generative model for it. We used inverse-transform sampling to generate data from the estimated conditional distribution through the fitted VQR model,  $\hat{Q}_{\mathbf{Y}|\mathbf{X}}(\mathbf{u}; \mathbf{x})$ , as follows.

1. Sample  $L$  evaluation covariate vectors,  $\{\mathbf{x}_l\}_{l=1}^L$  values at random from the ground truth distribution  $P_{\mathbf{X}}$ .
2. For each  $\mathbf{x}_l$ ,
  - (a) Sample  $M$  quantile levels  $\{\mathbf{u}_{m,l}\}_{m=1}^M$  uniformly.
  - (b) Generate  $M$  samples from the estimated distribution of  $\mathbf{Y}|\mathbf{X}$  using the estimated CVQF:  $\{\hat{\mathbf{y}}_{m,l} = \hat{Q}_{\mathbf{Y}|\mathbf{X}}(\mathbf{u}_{m,l}; \mathbf{x}_l)\}_{m=1}^M$ .
  - (c) Sample an additional  $M$  points  $\{\mathbf{y}_{m,l}^*\}_{m=1}^M$  from the ground truth conditional distribution  $P_{\mathbf{Y}|\mathbf{X}=\mathbf{x}_l}$ .
  - (d) Calculate a Kernel Density Estimate (KDE)  $\hat{f}_{\mathbf{Y}|\mathbf{X}=\mathbf{x}_l}$  from the VQR samples  $\{\hat{\mathbf{y}}_{m,l}\}$ .
  - (e) Calculate the KDE  $f_{\mathbf{Y}|\mathbf{X}=\mathbf{x}_l}^*$  from the ground truth samples  $\{\mathbf{y}_{m,l}^*\}$ .
3. Calculate the KDE-L1 metric as
$$\frac{1}{L} \sum_{l=1}^L \left\| f_{\mathbf{Y}|\mathbf{X}=\mathbf{x}_l}^* - \hat{f}_{\mathbf{Y}|\mathbf{X}=\mathbf{x}_l} \right\|_1.$$

The KDEs are calculated with 100 bins per dimension. An isotropic Gaussian kernel was used, with  $\sigma = 0.1$  for the conditional-banana dataset and  $\sigma = 0.035$  for the star dataset. We used `pykeops` [8] for a fast implementation of high-dimensional KDEs. We used  $L = 20$  and  $M = 4000$ .

**Quantile function distance (QFD).** This metric measures the distance between a true CVQF,  $Q_{\mathbf{Y}|\mathbf{X}}^*$ , and an estimate for it obtained by VQR,  $\hat{Q}_{\mathbf{Y}|\mathbf{X}}$ .

1. Sample  $L$  evaluation covariate vectors,  $\{\mathbf{x}_l\}_{l=1}^L$  values at random from the ground truth distribution  $P_{\mathbf{X}}$ .
2. For each  $\mathbf{x}_l$ ,
  - (a) Sample  $M$  points  $\{\mathbf{y}_{m,l}\}_{m=1}^M$  from the ground truth conditional distribution  $P_{\mathbf{Y}|\mathbf{X}=\mathbf{x}_l}$ .

Table 2: Quantitative evaluation of linear VQR and nonlinear VQR on the rotating stars dataset. Evaluated on  $N = 4000$  samples with  $T = 50$  levels per dimension. The KDE-L1, QFD and Entropy metrics are defined in section 6. Arrows  $\uparrow/\downarrow$  indicate when higher/lower is better; Numbers are mean  $\pm$  st.d. Reference entropy is obtained by uniformly sampling the 2d quantile grid.

		VQR	NL-VQR
KDE-L1	$\downarrow$	$0.35 \pm 0.06$	<b><math>0.20 \pm 0.01</math></b>
Quantile Function Distance (QFD)	$\downarrow$	$0.18 \pm 0.04$	<b><math>0.08 \pm 0.01</math></b>
Inverse CVQF Entropy (Ref: 0.69)	$\uparrow$	$0.51 \pm 0.02$	<b><math>0.59 \pm 0.02</math></b>
Train time (min)	$\downarrow$	<b>3.5</b>	4

- (b) Estimate an unconditional vector quantile function on  $\{\mathbf{y}_{m,l}\}_{m=1}^M$ , i.e. perform vector quantile estimation, not regression. Denote the estimated unconditional vector quantile function as  $Q_{\mathbf{Y}|\mathbf{X}}^*$ . This serves as a proxy for the ground-truth conditional quantile function.
- (c) Denote the estimated conditional quantile function evaluated at  $\mathbf{x}_l$ :  $\hat{Q}_{\mathbf{Y}|\mathbf{X}=\mathbf{x}_l}$ .
- (d) Compute the normalized difference between them elementwise over each of the  $T^d$  discrete quantile levels, i.e.,

$$d_l = \left\| Q_{\mathbf{Y}|\mathbf{X}=\mathbf{x}_l}^* - \hat{Q}_{\mathbf{Y}|\mathbf{X}=\mathbf{x}_l} \right\|_2 / \left\| Q_{\mathbf{Y}|\mathbf{X}=\mathbf{x}_l}^* \right\|_2.$$

- 3. Calculate the QFD metric as  $\frac{1}{L} \sum_{l=1}^L d_l$ .

We used  $L = 20$  and  $M = 4000$ .

**Percentage of co-monotonicity violations (MV).** This value can be measured directly. Given an estimated vector quantile function  $\hat{Q}(\mathbf{u})$ , with  $T$  levels per dimension, there are in total  $T^{2d}$  quantile level pairs. Thus, we measure

$$\frac{1}{T^{2d}} \sum_{i,j}^{T^d} \mathbb{I} \left\{ (\mathbf{u}_i - \mathbf{u}_j)^\top (\hat{Q}(\mathbf{u}_i) - \hat{Q}(\mathbf{u}_j)) < 0 \right\}.$$

### C.3 Scale and Optimization

We provide additional experiment results to showcase performance of our solver with respect to additional parameters. Figure 6 shows our solver’s runtime with respect to the number of target dimensions  $d$  and covariate dimensions  $k$ . Figure 7 shows the effect of the regularization strength parameter,  $\varepsilon$  on the accuracy of the solution.

### C.4 VMR

Figure 8 shows the effectiveness of our VMR procedure. We can see that when applying VMR, there are no monotonicity violations, even for low values of  $\varepsilon$ , and, moreover, QFD metric improves. In addition, figs. 9b and 9c demonstrate how VMR can remove monotonicity violations, even when the distribution cannot be estimated correctly (in this case due to linear VQR).

### C.5 Nonlinear VQR

Here we include additional results comparing linear and nonlinear VQR for various datasets. Figure 9c compares linear and nonlinear VQR on the synthetic glasses dataset. Figures 10 and 11 and table 2 present the results of linear and nonlinear VQR on the conditional-banana and rotating star datasets for many values of  $\mathbf{x}$ .

## D Implementation details

**Solver implementation details.** Of note are two key details for the SGD-based VQR solver (section 3) to converge.

- Equations (5) and (7) assume zero-mean covariates, thus when SGD is performed it is crucial to ensure that the sampled  $\mathbf{x}$ ’s are of zero mean.

- The log-sum-exp term in eq. (7) becomes numerically unstable as  $\varepsilon$  decreases, which can be mitigated by implementing it as

$$\text{logsumexp}_\varepsilon(\mathbf{x}) = \text{logsumexp}_\varepsilon \left( \mathbf{x} - \max_k \{x_k\} \right) + \max_k \{x_k\}.$$

**Scale and Optimization experiment details.** For both scale and optimization experiments, we run VQR for  $10k$  iterations and use a learning rate scheduler that decays the learning rate by a factor of 0.9 every 500 iterations if the error does not drop by 0.5%.

**Synthetic glasses experiment details.** We set  $N = 10k$ ,  $T = 100$ , and  $\varepsilon = 0.001$ . We optimized both VQR and NL-VQR for  $40k$  iterations and use a learning rate scheduler that decays the learning rate by a factor of 0.9 every 500 iterations if the error does not drop by 0.5%. In NL-VQR, as  $g_\theta$ , we used a 3-layer fully-connected network with each hidden layer of size 1000. We used skip-connections, batch-norm, and ReLU nonlinearities between the hidden layers. For NL-VQR and VQR, we set the initial learning rate to be 0.4 and 1, respectively.

**Cond-banana and rotating star experiment details.** We set  $N = 20k$ ,  $T = 50$ ,  $\varepsilon = 0.005$ . We optimized both VQR and NL-VQR for  $20k$  iterations. We used the same learning rate and schedulers as in the synthetic glasses experiment. For NL-VQR, we set  $g_\theta$  to be a small 3-layer fully-connected network with hidden layer sizes to be  $(2, 10, 20)$  with ReLU nonlinearities.

**Machine configuration.** All experiments were run on a machine with an Intel Xeon E5 CPU, 256GB of RAM and an Nvidia Titan 2080Ti GPU with 11GB dedicated graphics memory.

## E Software

We provide our VQR solvers as part of a comprehensive python package, which will be published to github upon publication. The supplementary material contains compiled jupyter notebooks which demonstrate the use of our package.

**Existing VQR implementation.** Although a reference matlab implementation of linear VQR by the original authors exists<sup>7</sup>, this implementation is regarded by the authors as being in “alpha” stage (i.e., not for general use). Moreover, it relies on solving the exact formulation (eq. (5)) using a general-purpose linear program solver. Feldman et al. [12] found it to be prohibitively slow even for small problems, and noted runtimes of over an hour for  $N = 10k$ ,  $d = 2$ ,  $k = 50$ ,  $T = 32$ . Thus, this implementation was deemed unsuitable for large problems. For comparison, our solver converges to a useful solution on a problem of this size in less than one minute.

---

<sup>7</sup><https://github.com/alfredgalichon/VQR>

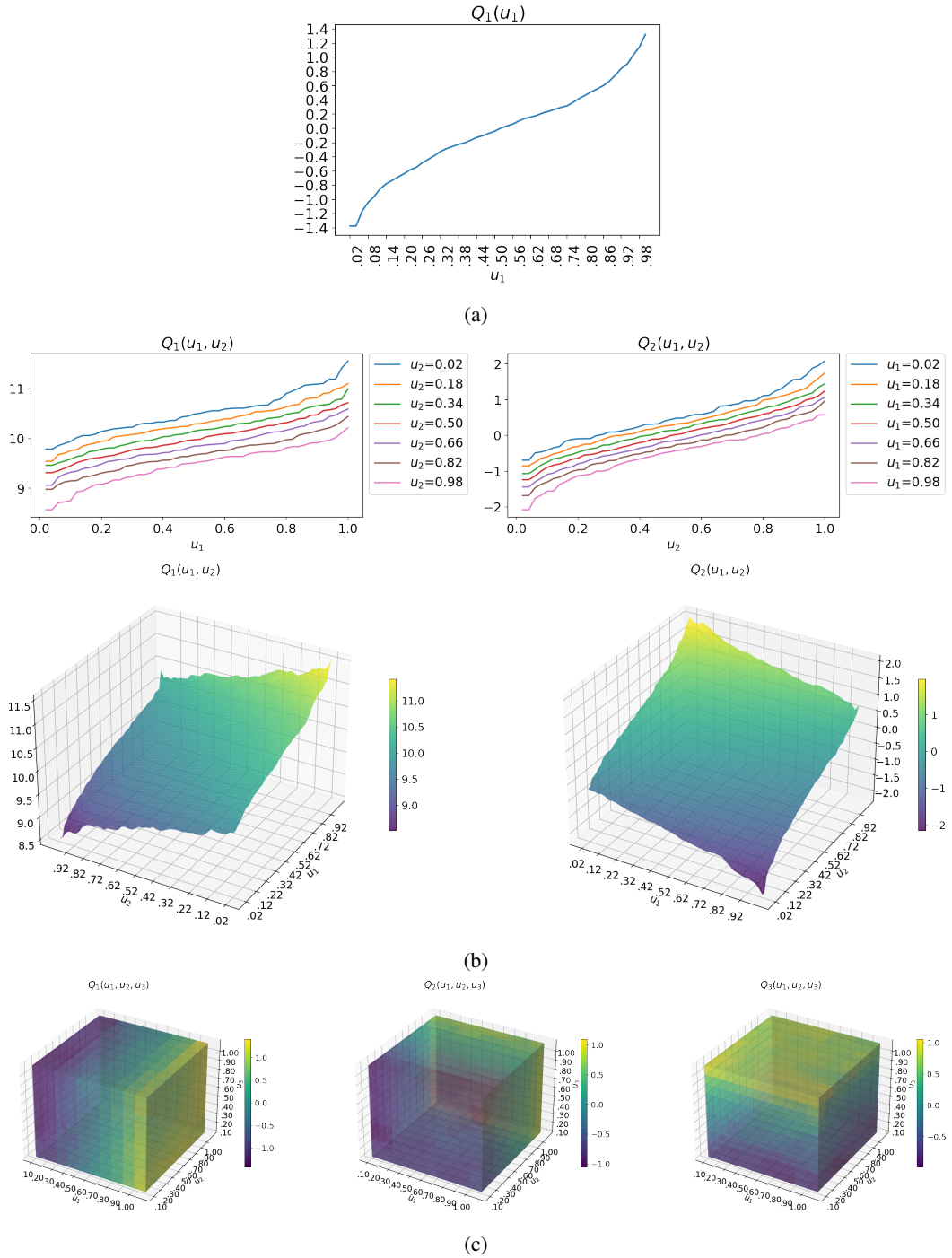


Figure 5: Example of (a) 1d, (b) 2d, and (c) 3d vector quantiles estimated on the MVN dataset. In each plot,  $Q_i(\mathbf{u})$  is the  $i$ th component of the vector quantile  $\mathbf{Q}_Y(\mathbf{u})$ , plotted over all quantile levels  $\mathbf{u}$ . The number of quantile levels calculated was 50, 25 and 10 for 1d, 2d and 3d quantiles respectively. For 2d quantiles (b), the top plot shows multiple monotonic quantile curves of one variable while keeping the other at a fixed level.

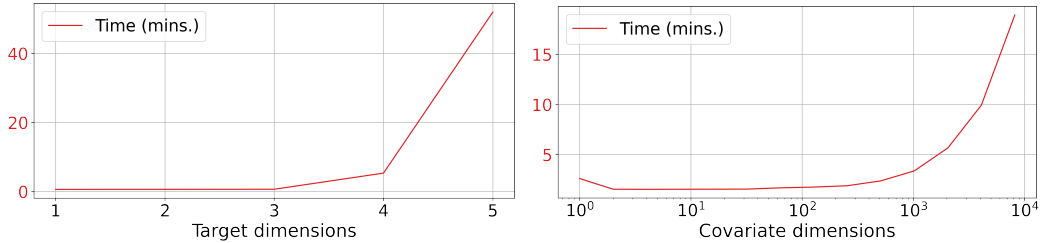


Figure 6: VQR solver runtime as a function of number of target dimensions  $d$  (left) and covariate dimensions  $k$  (right). Calculated on the MVN dataset with  $N = 10k$ ; for  $d$  experiment  $T = 10$ ; for  $k$  experiment  $T = 50$  and  $d = 2$ . Runtime scales exponentially with  $d$  as expected, due to having  $T^d$  quantile levels. For  $k$ , we can see that runtime remains relatively constant even for hundreds of dimensions, then starts to increase due to memory constraints.

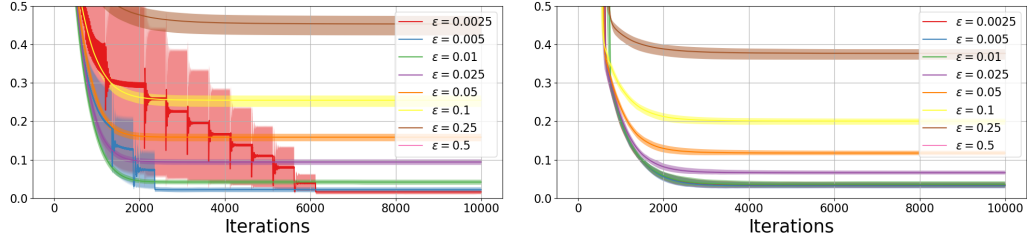


Figure 7: Effect of epsilon on strong representation, quantified by the QFD metric. Calculated on the MVN dataset with  $N = 20k$ ,  $k = 1$ . Right:  $T = 50$ ,  $d = 2$ . Left:  $T = 100$ ,  $d = 1$ . As epsilon decreases, the relaxed dual (7) becomes more exact. This is reflected here in the QFD metric, the final value of which decreases as  $\varepsilon$  decreases.

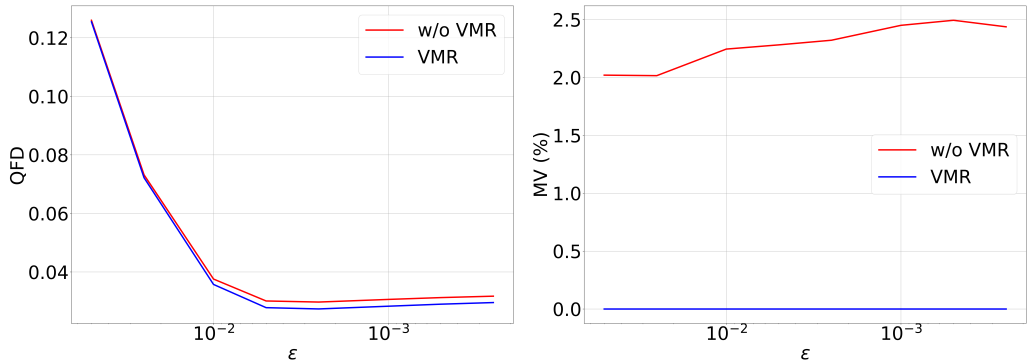


Figure 8: Strong representation and monotonicity as a function of  $\varepsilon$ , with and without VMR. VMR improves the final value of the QFD (left), and completely eliminates monotonicity violations (right). Without VMR, the number of monotonicity violations increases (right, red) as the problem becomes more exact (smaller  $\varepsilon$ ). This demonstrates that by using VMR, we can use lower values of  $\varepsilon$  to obtain a more accurate solution (better QFD) without compromising monotonicity. Calculated on the MVN dataset with  $N = 20k$ ,  $T = 50$ ,  $d = 2$ ,  $k = 1$ .

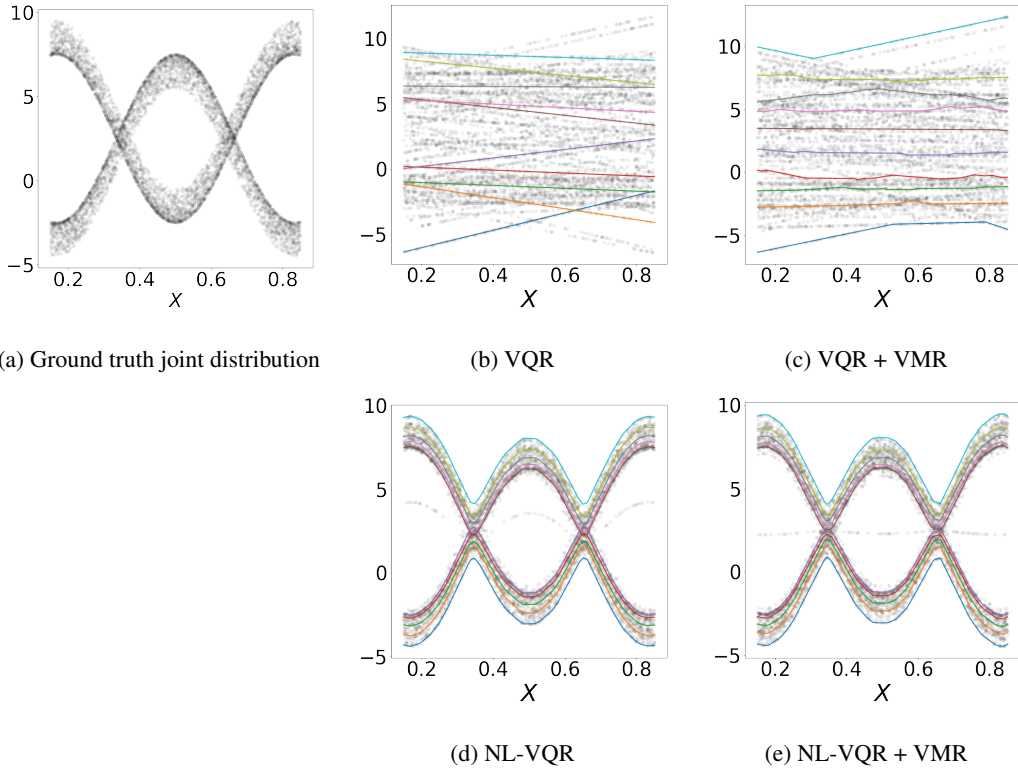


Figure 9: SQR on the synthetic glasses dataset (a; gray points show ground-truth distribution). Linear VQR fails to correctly model the conditional distribution (b, c; gray points sampled from linear VQR), while nonlinear VQR reconstructs the shape exactly (d, e; gray points sampled from nonlinear VQR). In either case, VMR successfully eliminates any quantile crossings (c, e).

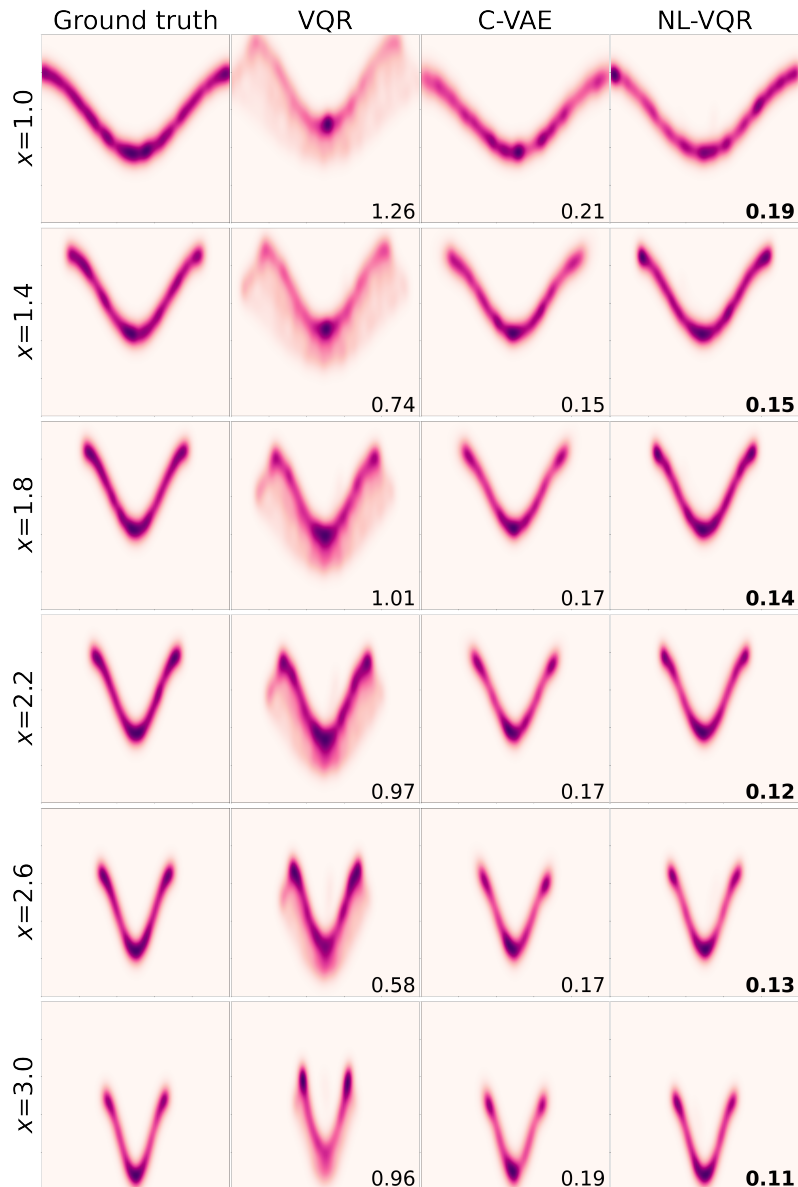


Figure 10: Comparison of kernel-density estimates of samples drawn from linear VQR and nonlinear VQR (NL-VQR), trained on the conditional-banana dataset. Models were trained with  $N = 20k$  with  $T = 50$  quantile levels per dimension. Numbers depict the KDE-L1 metric. Better viewed as GIF provided in the supplementary material.

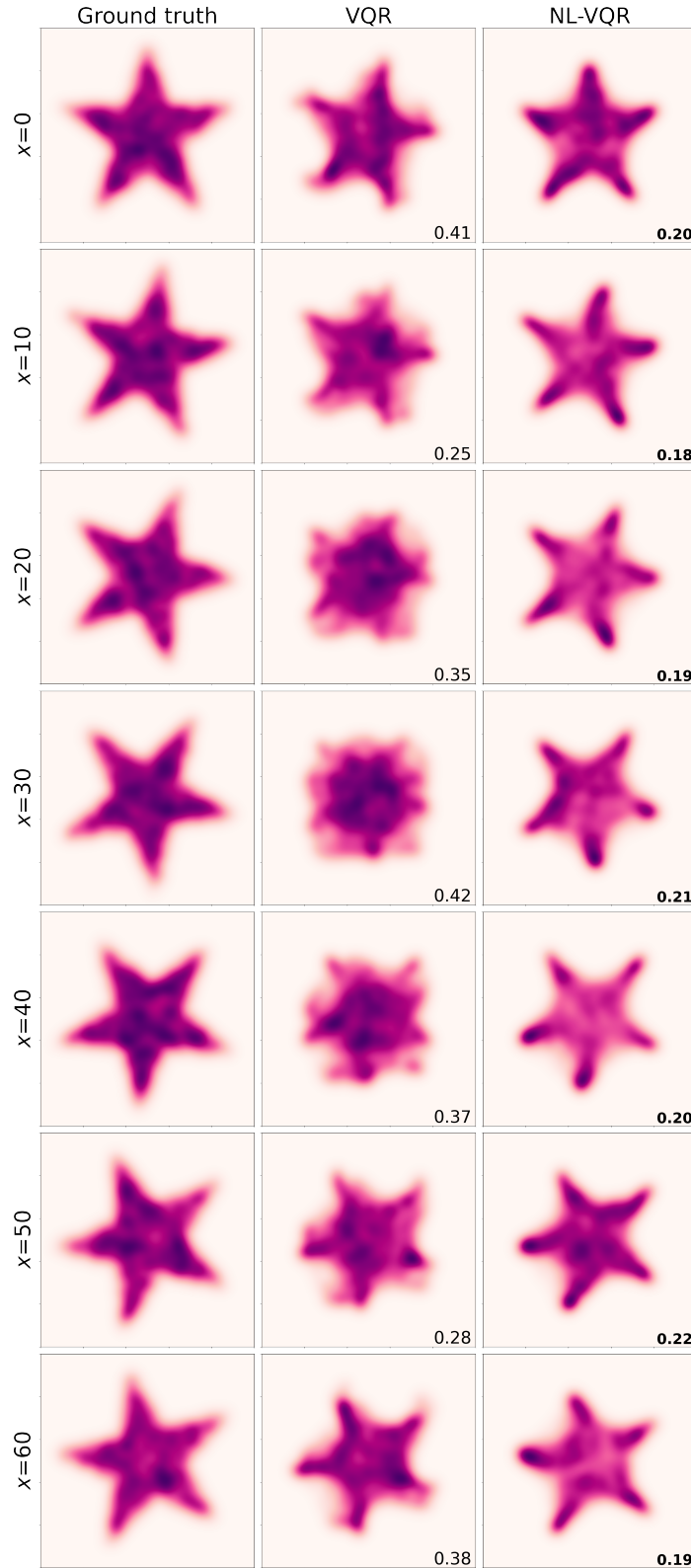


Figure 11: Comparison of kernel-density estimates of samples drawn from linear VQR and nonlinear VQR (NL-VQR), trained on the rotating star dataset. Models were trained with  $N = 20k$  with  $T = 50$  quantile levels per dimension. Numbers depict the KDE-L1 metric. Better viewed as GIF provided in the supplementary material.